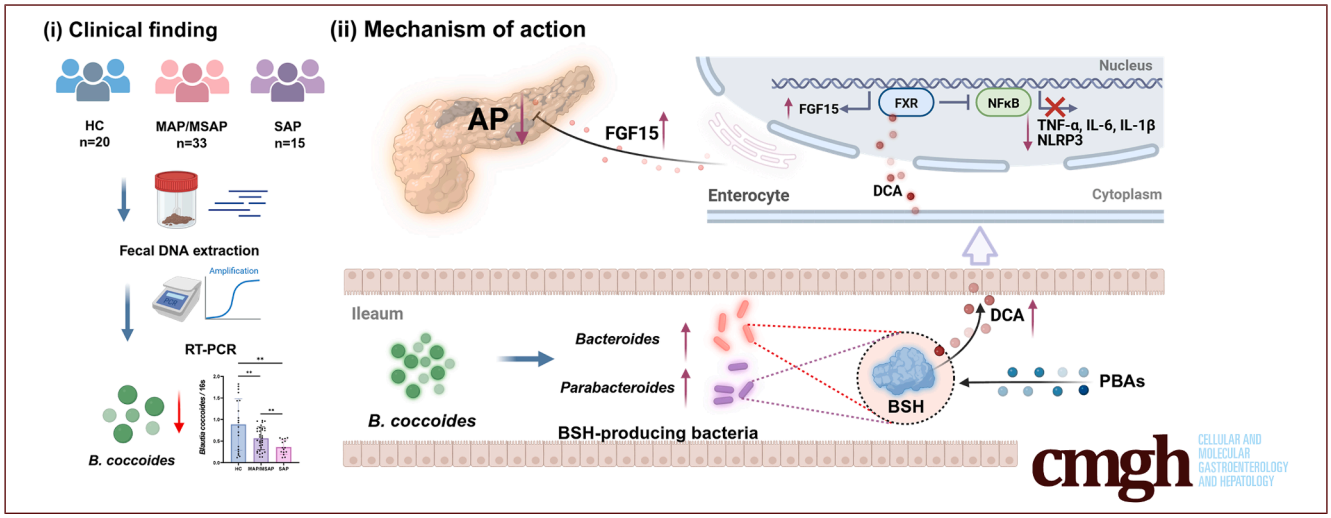
cmgh
CELLULAR AND MOLECULAR GASTROENTEROLOGY AND HEPATOLOGY

ORIGINAL RESEARCH

Blautia coccoides Alleviates Acute Pancreatitis via Bile Salt Hydrolase-mediated Deoxycholic Acid Production and Farnesoid X Receptor Signaling

Yang Fu,[1,2,3,*] Binqiang Xu,[1,2,*] Wenfei Qin,[4,*] Wei Xiao,[5] Huizhen Huang,[1,2] Jia Hu,[1,2] Mengyan Cui,[1,2] Qixiang Mei,[1,2] Junjie Fan,[1,2] Chunlan Huang,[1,2] and Yue Zeng[1,2]

[1]*Department of Gastroenterology, Shanghai General Hospital, Shanghai Jiao Tong University School of Medicine, Shanghai, China;* [2]*Institute of Pancreatic Diseases, Shanghai Jiao Tong University School of Medicine, Shanghai, China;* [3]*Department of Gastroenterology, Northern Jiangsu People's Hospital Affiliated to Yangzhou University, Yangzhou, China;* [4]*School of Agriculture and Biology, Shanghai Jiao Tong University, Shanghai, China; and* [5]*School of Health Science and Engineering, Shanghai Engineering Research Center of Food Microbiology, University of Shanghai for Science and Technology, Shanghai, China*



SUMMARY

We identify *Blautia coccoides* as a protective gut commensal in acute pancreatitis. It reshapes the microbiota to increase bile salt hydrolase-dependent deoxycholic acid, activates farnesoid X receptor-fibroblast growth factor 15 signaling, and alleviates the severity of acute pancreatitis.

BACKGROUND & AIMS: Gut dysbiosis is involved in the pathogenesis of acute pancreatitis (AP), yet therapeutic interventions remain limited. Our previous study found the relative abundance of *Blautia* is significantly decreased in AP, suggesting its protective role.

METHODS: We quantified *Blautia coccoides* in patients with AP and tested its effects in AP mice. Untargeted metabolomics identified deoxycholic acid. Farnesoid X receptor (FXR) signaling was tested with agonists and antagonists. 16S rRNA sequencing was applied to explore changes of gut microbiota. In vitro co-culture assays verified the microbial interaction. The role of bile salt hydrolase (BSH) was confirmed through experiments involving inhibitor and BSH-engineered *E coli*.

WHAT YOU NEED TO KNOW

Background: Gut dysbiosis is involved in acute pancreatitis (AP), yet therapies remain limited. We investigated the role of *Blautia coccoides*, which is depleted in patients with AP, to understand its underlying mechanisms.

Impact: We identified that *B coccoides* alleviates AP by reshaping gut microbiota to enhance bile salt hydrolase-mediated deoxycholic acid production. This activates the intestinal Farnesoid X receptor-fibroblast growth factor 15 pathway, effectively suppressing inflammation and protecting pancreatic tissue.

Future Directions: Our findings highlight the therapeutic potential of gut microbiota and bile acid metabolism. Future clinical strategies could leverage *B coccoides* or its downstream metabolites to effectively treat AP.

RESULTS: We observed reduced *B coccoides* in patients with AP that correlated with disease severity. In AP mice, gavage of *B coccoides* mitigated pancreatic and intestinal injury. Untargeted metabolomics revealed the increased level of

deoxycholic acid (DCA), which could reproduce the protective phenotype of *B coccoides*. We further found that DCA acts primarily within the intestine to activate FXR, which suppressed pro-inflammatory nuclear factor κB (NF-κB) and NLRP3 pathways. FXR activation also induced production of fibroblast growth factor 15 (FGF15), which protected pancreatic acinar cells. 16S rRNA sequencing showed that *B coccoides* increased the abundance of BSH-producing genera, *Parabacteroides* and *Bacteroides*. In vitro, *B coccoides* supernatant promoted the growth of representative strains from these genera. Inhibition of BSH abrogated the protective effects of *B coccoides*, whereas administration of BSH-engineered *E coli* could ameliorate AP.

CONCLUSIONS: *B coccoides* alleviated AP by reshaping gut microbiota composition, enhancing BSH-mediated DCA production, and activating the intestinal FXR–FGF15 signaling to suppress inflammation. *(Cell Mol Gastroenterol Hepatol 2026;20:101732; https://doi.org/10.1016/j.jcmgh.2026.101732)*

Keywords: Acute Pancreatitis; Bile Salt Hydrolase; *Blautia coccoides*; Deoxycholic Acid; Farnesoid X Receptor.

This article has an accompanying Editorial.

Acute pancreatitis (AP) is a common gastrointestinal emergency with a rising global incidence, and approximately 20% of cases progress to severe acute pancreatitis (SAP) with a mortality rate as high as 30%.[1,2] Recent insights into AP pathogenesis have shifted from the local inflammation to an understanding of AP as a systemic disease, driven by complex crosstalk between the pancreas and distal organs via dysregulated metabolic signaling molecules such as long- and short-chain fatty acids (SCFAs), tryptophan metabolites, and bile acids (BAs).[3–7] Notably, the metabolism of BAs underwent significant changes in patients with AP.[8] It has been reported that serum profiles of primary BAs (PBAs), particularly chenodeoxycholic acid (CDCA) and cholic acid (CA), are markedly decreased during AP.[8] Supplementation with CDCA has shown protection against acinar cell necrosis through the Farnesoid X receptor (FXR) and modulation of mitochondrial function. In addition, some secondary BAs (SBAs), such as tauroursodeoxycholic acid (TUDCA) and dehydrocholic acid, also exert protective effects in experimental AP.[9,10]

PBAs, synthesized from cholesterol in hepatocytes, are subsequently converted into SBAs by the gut microbiota, linking this transformation intimately to both microbial composition and host metabolism.[11] The initial microbial modification is the deconjugation of PBAs, a reaction catalyzed by bile salt hydrolase (BSH).[12] BSH activity is widespread among commensal genera such as *Bacteroides, Bifidobacterium*, and *Lactobacillus*.[12] Following deconjugation, free PBAs are further transformed into SBAs through the 7α-dehydroxylase, which can be produced only by a few bacteria such as *Clostridium scindens*.[13] Therefore, the balance of the BA pool can be disrupted by gut dysbiosis through altering these crucial enzymatic activities, leading to a proinflammatory state that is implicated in various gastrointestinal diseases.[11] However, the role of microbiota-mediated BA metabolism in the pathogenesis of AP remains unclear.

Our previous research illustrated that reduction of *Blautia* abundance is implicated in the pathogenesis of AP and closely linked to dysfunction of ileal Paneth cells, the primary producers of antimicrobial peptides.[14] *Blautia*, a common inhabitant of gut microbiota, is increasingly recognized for its beneficial functions, including the alleviation of metabolic syndrome and inflammatory diseases, and exerting antibacterial effects against specific pathogens.[15] Because some *Blautia* species, such as *B obeum* and *B hansenii*, encode BSH that could deconjugate BAs, the noticeable decline of this functionally relevant genus in AP suggests it may be an important target for further study.[12]

The objective of this study was to investigate the ameliorating effect of *Blautia* in AP and to elucidate its underlying mechanisms. A detailed understanding of the interaction

***Authors share co-first authorship.**

Abbreviations used in this paper: **Angptl4, angiopoietin-like protein 4; ANOVA, analysis of variance; AP, acute pancreatitis; APACHE II, Acute Physiology and Chronic Health Evaluation II; ASFV, African swine fever virus; ASV, amplicon sequence variant; AUC, area under the curve; BAs, bile acids; BcAP, *Blautia coccoides* acute pancreatitis; BHI, brain heart infusion; BISAP, Bedside Index for Severity in Acute Pancreatitis; BMI, body mass index; BSA, bovine serum albumin; BSH, bile salt hydrolase; CA, cholic acid; CCK, cholecystokinin; CDCA, chenodeoxycholic acid; CFU, colony forming units; COG, Clusters of Orthologous Genes/Groups; CON, control; CRP, C-reactive protein; DAB, diaminobenzidine; DAO, diamine oxidase; DAPI, 4′,6-diamidino-2-phenylindole; DCA, deoxycholic acid; DMEM, Dulbecco's Modified Eagle Medium; DSS, dextran sodium sulfate; ELISA, enzyme-linked immunosorbent assay; ESI, electrospray ionization; FBS, fetal bovine serum; FGF15, fibroblast growth factor 15; FISH, fluorescence in situ hybridization; FMT, fecal microbiota transplantation; FXR, Farnesoid X receptor; GR-7, Gut Restricted-7; H&E, hematoxylin and eosin; HC, healthy controls; HILIC, hydrophilic interaction liquid chromatography; HRP, horseradish peroxidase; IACUC, Institutional Animal Care and Use Committee; IF, immunofluorescence; IHC, immunohistochemistry; IL, interleukin; IQR, interquartile range; KEGG, Kyoto Encyclopedia of Genes and Genomes; LB, Lysogeny broth; LCA, lithocholic acid; LC-MS, Liquid chromatography-mass spectrometry; LDH, lactate dehydrogenase; LPS, lipopolysaccharide; MAP, mild acute pancreatitis; MRS, DeMan, Rogosa, and Sharpe; MSAP, moderately severe acute pancreatitis; NCBI, National Center for Biotechnology Information; NF-κB, nuclear factor κB; PAC, pancreatic acinar cell; PASS, Pancreatitis Activity Scoring System; PBAs, primary bile acids; PBS, phosphate-buffered saline; PCoA, principal coordinates analysis; PCR, polymerase chain reaction; PGE2, prostaglandin E2; PI, propidium iodide; PLS-DA, partial least squares discriminant analysis; PVDF, polyvinylidene fluoride; ROC, receiver operating characteristic; SAP, severe acute pancreatitis; SBAs, secondary bile acids; SCFA, short-chain fatty acid; SDS-PAGE, sodium dodecyl sulfate-polyacrylamide gel electrophoresis; SEM, standard error of the mean; SPF, specific pathogen-free; TBST, Tris-buffered saline with Tween 20; TNF-α, tumor necrosis factor alpha; TOF-MS, time of flight mass spectometry; TUDCA, tauroursodeoxycholic acid; TUNEL, terminal deoxynucleotidyl transferase dUTP nick-end labeling; UHPLC, ultra-high-performance liquid chromatography; VIP, Variable Importance in Projection; WBC, white blood cells.**

Most current article

© 2026 The Authors. Published by Elsevier Inc. on behalf of the AGA Institute. This is an open access article under the CC BY-NC-ND license (http://creativecommons.org/licenses/by-nc-nd/4.0/).

2352-345X
https://doi.org/10.1016/j.jcmgh.2026.101732

between *Blautia*, BA metabolism, and inflammation could provide the basis for therapeutic targets in the treatment of AP.

Results

B coccoides *Alleviated AP*

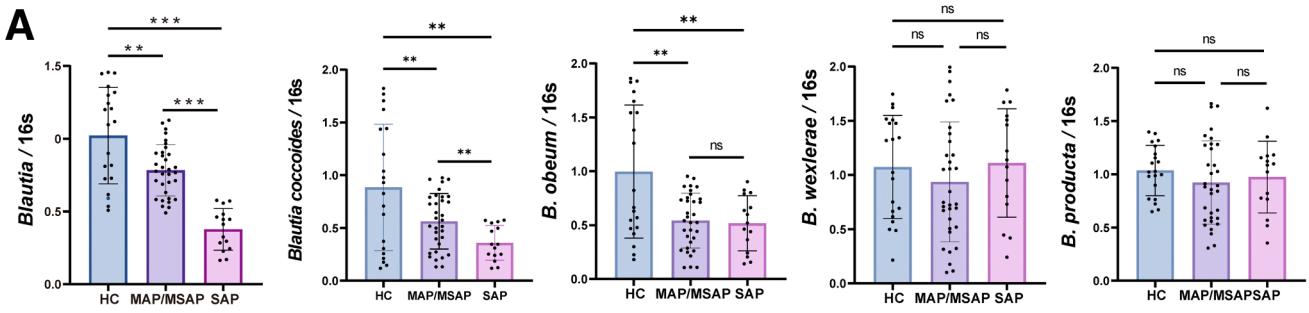
Based on our previous findings of altered *Blautia* abundance in AP mice, we sought to validate these observations in patients with AP.[14] Fecal samples from 33 patients with mild AP (MAP)/moderately severe AP (MSAP), 15 patients with SAP, and 20 healthy controls (HCs) were harvested. The baseline characteristic profiles (age, sex, and body mass index [BMI]) showed no statistical differences among these 3 groups (Table 1). Compared with the HC group, *Blautia* relative abundance significantly decreased in the MAP/MSAP group and was further reduced in the SAP group (Figure 1*A*). We then quantified the relative abundance of 4 common *Blautia* species in the gut microbiota of humans, including *B obeum*, *B coccoides*, *B producta*, and *B wexlerae* by real-time polymerase chain reaction (PCR). *B coccoides* abundance had a stepwise decline in patients with AP, consistent with disease severity, and a significantly negative relation with laboratory indicators and clinical disease scoring systems (Acute Physiology and Chronic Health Evaluation II [APACHE II], Bedside Index for Severity in Acute Pancreatitis [BISAP], Pancreatitis Activity Scoring System [PASS], and Ranson scores), whereas other *Blautia* species showed no similar trend or correlations (Figure 1*A* and *B*).

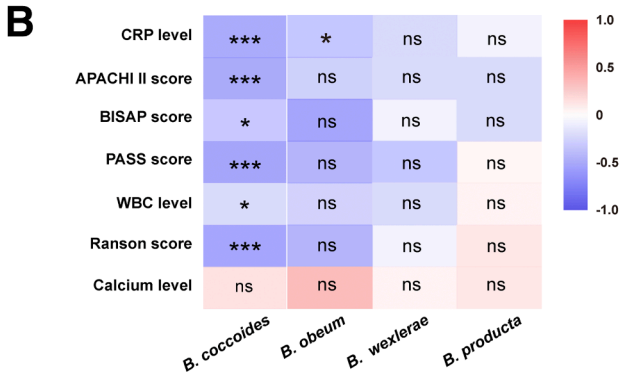
To validate potential protective effects of *Blautia* in AP, mice were gavaged with *B coccoides* for 28 days before cerulein and lipopolysaccharide (LPS) induction (BcAP) (Figure 1*C*). Gavage of *B coccoides* markedly attenuated pancreatic histopathological injury (Figure 1*D*) and serum amylase activity (Figure 1*E*) in AP mice. Compared with the AP group, pancreatic pro-inflammatory cytokines (tumor necrosis factor alpha [TNF-α], interleukin [IL]-6, and IL-1β) and acinar cell apoptosis were significantly downregulated in the BcAP group (Figure 1*F* and *G*). Gut barrier dysfunction was also evaluated in the BcAP group. The ileal damage, inflammation, and apoptosis of epithelial cells was markedly attenuated (Figure 2*A*–*C*). Serum D-lactate and diamine oxidase (DAO) levels decreased, and tight junction proteins (ZO-1 and Claudin-1) were restored (Figure 2*D* and *E*). Bacterial translocation following the impaired

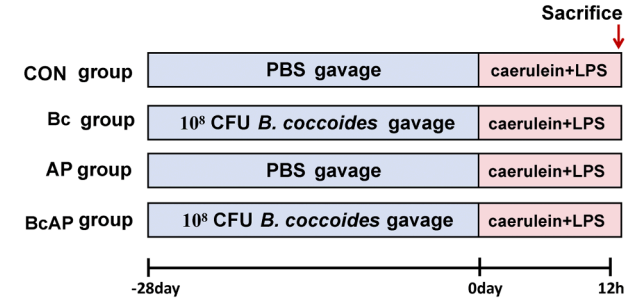
Table 1. Clinical and Demographic Characteristics

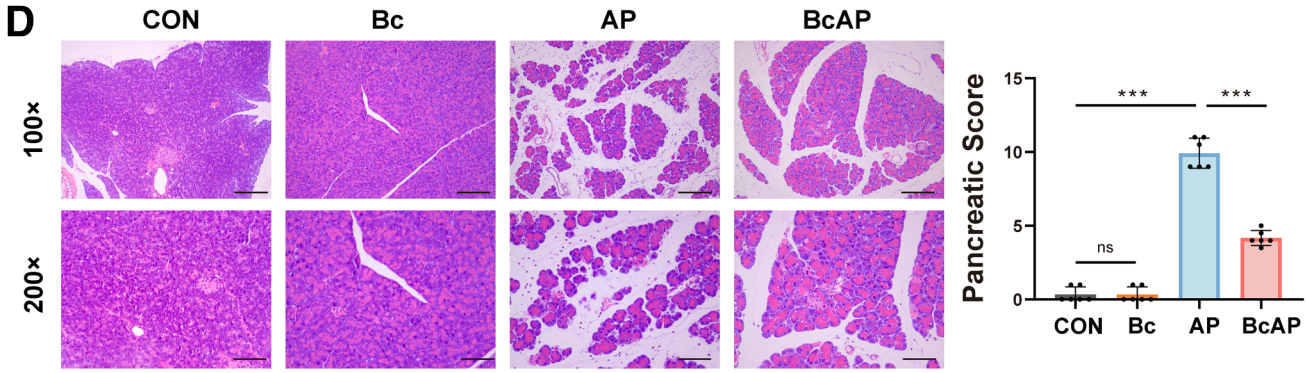
Parameters	AP		HCs (n = 20)	*P* value
	MAP/MSAP (n = 33)	SAP (n = 15)		
Male	17 (51.51)	10 (66.67)	11 (55)	.342[a] .639[b]
Age, *y*	45.67 (6.54)	40.50 (7.56)	50.20 (8.01)	.367[a] .211[b]
BMI, kg/m^2	24.78 (2.98)	25.61 (2.47)	23.29 (2.69)	.311[a] .161[b]
Disease etiology				
Gallstones-related	17 (51.51)	7 (46.67)	–	.612[a]
Hypertriglyceridemia	14 (42.42)	7 (46.67)	–	.589[a]
Alcoholic	2 (6.06)	1 (6.67)	–	.298[a]
CRP, *mg/L*	57.90 (14.38–76.59)	145.60 (119.5–161.2)	–	<.001[a]
APACHI II score	2 (1–3)	7 (6–8)	–	<.001[a]
BISAP score	0 (0–1)	1 (1–2)	–	<.001[a]
PASS score	60 (32.5–130)	170 (160–185)	–	<.001[a]
WBC, $\times 10^9/L$	11.5 (10.55–12.7)	12.90 (12–14.1)	–	.021[a]
Calcium, *mmol/L*	2.37 (0.07)	2.27 (0.2)	–	.013[a]
Ranson score	0 (0–1)	3 (2–4)	–	<.001[a]
Local complications	9 (27.27)	10 (66.67)	–	<.001[a]
SIRS	13 (39.39)	9 (60)	–	<.001[a]
Hypertension	9 (27.27)	5 (33.33)	5 (25)	.738[a] .999[b]
Diabetes	12 (36.36)	6 (40)	6 (30)	.592[a] .999[b]

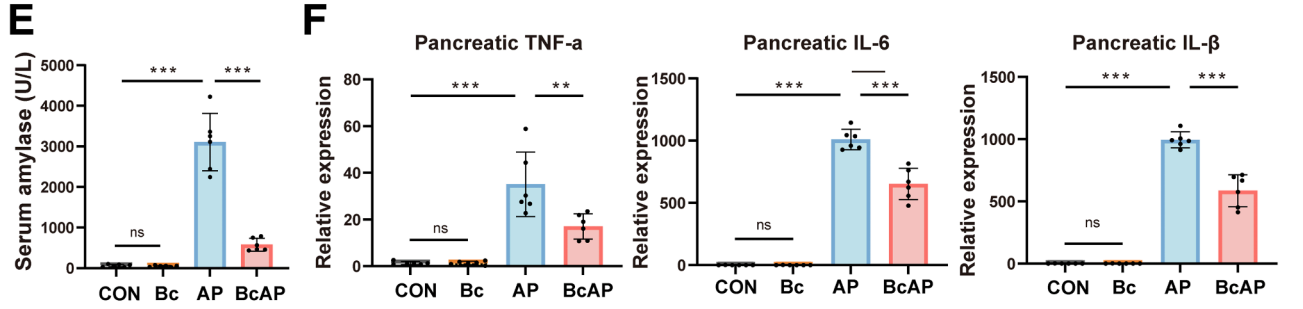
NOTE. Data are presented as number (%), mean (standard deviation), or median (interquartile range).
AP, acute pancreatitis; APACHE II, Acute Physiology and Chronic Health Evaluation II; BISAP, Bedside Index for Severity in Acute Pancreatitis; BMI, body mass index; CRP, C-reactive protein; HC, healthy controls; MAP, mild acute pancreatitis; MSAP, moderately severe acute pancreatitis; PASS, Pancreatitis Activity Scoring System; SAP, severe acute pancreatitis; SIRS, systemic inflammatory response syndrome; WBC, white blood cell.
[a]The MAP/MSAP group compared with the SAP group.
[b]The AP group (MAP/MSAP and SAP) compared with the HC group.

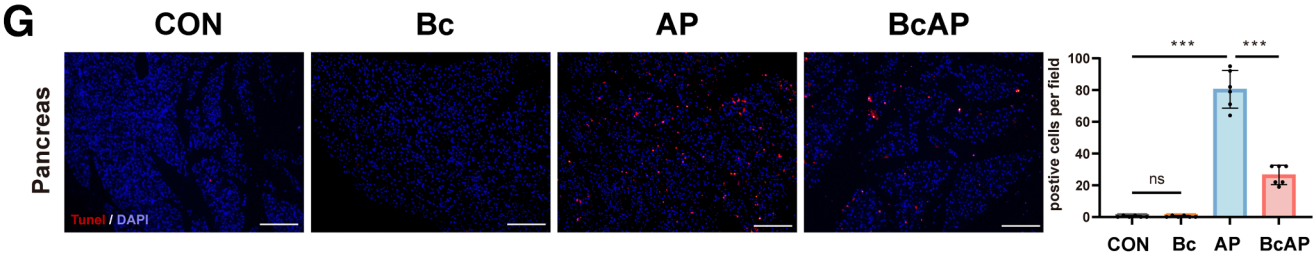

A
Blautia / 16s
Blautia coccoides / 16s
B. obeum / 16s
B. wexlerae / 16s
B. producta / 16s
HC
MAP/MSAP
SAP


B
CRP level
APACHI II score
BISAP score
PASS score
WBC level
Ranson score
Calcium level
B. coccoides
B. obeum
B. wexlerae
B. producta


C
Sacrifice
CON group
PBS gavage
caerulein+LPS
Bc group
10⁸ CFU B. coccoides gavage
AP group
BcAP group
-28day
0day
12h


D
CON
Bc
AP
BcAP
100×
200×
Pancreatic Score


E
Serum amylase (U/L)
F
Pancreatic TNF-a
Pancreatic IL-6
Pancreatic IL-β
Relative expression


G
CON
Bc
AP
BcAP
Pancreas
Tunel / DAPI
postive cells per field

intestinal barrier is a major cause of pancreatic tissue necrotic infection and subsequent sepsis in AP.[16] We demonstrated that bacterial translocation breaking through ileal epithelial cells to the pancreas was significantly abated in the BcAP group by using fluorescence in situ hybridization (FISH) (Figure 2*F*).

Bile Acid Metabolism Participated in the Protective Effect of B coccoides *in AP*

Non-targeted metabolomics of cecal contents was leveraged to identify metabolic alterations in BcAP mice. In partial least squares discriminant analysis (PLS-DA) and volcano plot analysis, distinct metabolic profiles were illustrated from the control (CON) and Bc, AP and BcAP group, respectively (Figure 3*A*–*C*). SBAs biosynthesis as the most altered Kyoto Encyclopedia of Genes and Genomes (KEGG) pathway was also occurred (Figure 3*D* and *F*). Compared with AP, the top 5 differential metabolites ranked by Variable Importance in Projection (VIP) score were all BAs in the BcAP group (Figure 3*E* and *G*). Deoxycholic acid (DCA) significantly declined in AP mice, which was restored in the BcAP group (Figure 3*H*). These results implicated that BA metabolism might be involved in the protective mechanism of *B coccoides* against AP.

To verify the effect of DCA on AP, we then leveraged different dosages (1, 5, and 10 mg/kg DCA) on cerulein and LPS induction mice. Exogenous gavage of DCA relieved pancreatic pathological scores in a dose-dependent manner (Figure 4*A*). Compared with AP mice, serum amylase activity, pancreatic acinar cell apoptosis, and inflammation were significantly reduced in the DCA+AP group (Figure 4*B*–*D*). To the same extent, ileal integrity and tight junction proteins (ZO-1 and Claudin-1) were preserved, and ileal inflammation and bacterial translocation to the pancreas were also attenuated (Figure 4*E*–*J*). The elevation of fecal DCA may serve as a mechanistic link in alleviating AP.

FXR-Fibroblast Growth Factor 15 Signaling Pathway Was Activated in DCA-mediated Protection Against AP

Next, we aimed to elucidate the downstream signaling pathway activated by DCA in AP. In DCA+AP group, fecal DCA concentrations were the highest, with no significant changes in serum or pancreatic levels, indicating the intestine as the primary site of action (Figure 5*A*). Bile acids are known to signal through receptors like FXR and TGR5. Compared with CON mice, both ileal FXR and TGR5 expression were upregulated in AP mice, whereas only ileal FXR expression were increased in DCA+AP mice (Figure 5*B* and *C*). We further confirmed that expression of pancreatic FXR was unchanged in DCA+AP mice (Figure 5*D* and *E*).

Administration of an intestinal-specific FXR antagonist (Gly-β-MCA) in DCA+AP mice aggravates pancreatic and ileal injury (Figure 5*F*–*J*). Conversely, FXR agonist GW4064 significantly ameliorated pathological damage and reduced apoptosis in the pancreas and ileum in AP mice (Figure 5*F*–*I*). GW4064 also restored intestinal tight junction proteins (Figure 5*J*).

Fibroblast growth factor 15 (FGF15), an FXR target gene product, is known to signal from the intestine to the liver.[17] We found that, compared with AP mice, FGF15 was significantly elevated in serum and pancreas in DCA+AP mice and GW4064+AP mice, but was markedly diminished upon FXR inhibition (Figure 6*A*). Consistently, the pancreatic expression of the FGF15 receptor, FGFR4, was likewise upregulated by DCA or GW4060 and reduced by FXR inhibition (Figure 6*B*). In vitro, FGF15 significantly protected acinar cells from cholecystokinin (CCK) stimulation (Figure 6*C* and *D*) and reduced the expression of proinflammatory cytokines TNF-α, IL-6, and IL-1β (Figure 6*E*). All these protective effects of FGF15 were significantly diminished when co-treated with an FGFR4 inhibitor (Figure 6*C*–*E*), confirming the involvement of the FGF15-FGFR4 signaling pathway in mediating acinar cell protection. BAs also exert anti-inflammatory signaling function via the interaction of FXR with nuclear factor κB (NF-κB) and the NLRP3 inflammasome.[18,19] Phosphorylation of IκBα and p65 and NLRP3 protein expression were significantly reduced in the ileum of DCA+AP mice (Figure 6*F* and *G*). Similarly, in the ileum of BcAP mice, FXR expression was upregulated, and NF-κB and NLRP3 inflammasome pathways were inhibited (Figure 6*H* and *I*). Activation of FXR with GW4064 reproduced the reductions in intestinal p-IκBα, p-p65, and NLRP3 in AP mice, whereas DCA-mediated activation of FXR and the suppression of the NF-κB and NLRP3 pathways were markedly ablated by Gly-β-MCA (Figure 6*J* and *K*).

BSH-producing Bacteria Mediated the Regulation of BA Metabolism

The conversion of PBAs to SBAs is catalyzed exclusively by the gut microbiota via BSH and 7α-dehydroxylase. How does *B coccoides* administration lead to increased levels of DCA? We first applied an identical experiment using heat-inactivated *B coccoides* to explore whether the protective effect of *B coccoides* in AP depends on its metabolites. After heat inactivation, *B coccoides* showed no growth on the plates (Figure 7*A*). Heat-inactivated *B coccoides* failed to

Figure 1. (***See previous page***). ***B coccoides*** **mitigated pancreatic injuries in AP.** (*A*) Relative abundance of *Blautia*, *B coccoides*, *B obeum*, *B wexlerae*, *B producta* in patients with AP and HCs. (*B*) Correlation between the relative abundance of *B coccoides*, *B obeum*, *B wexlerae*, *B producta* and clinical indicators in patients with AP. (*C*) Schematic of the experimental procedure. (*D*) Histopathological changes and pathological scores of the pancreas. Original magnification, ×100 (top panels) or ×200 (bottom panels). (*E*) Serum amylase activity. (*F*) Real-time PCR analysis of TNF-α, IL-6, IL-1β mRNA level in pancreas; Tubulin was used as the reference gene. (*G*) TUNEL staining and quantification of TUNEL + cell in pancreas. Original magnification, ×200. The data are presented as the means ± SEM (n = 6 mice per group). $^{*}P < .05$; $^{**}P < .01$; $^{***}P < .001$. Bc, *Blautia coccoides*.

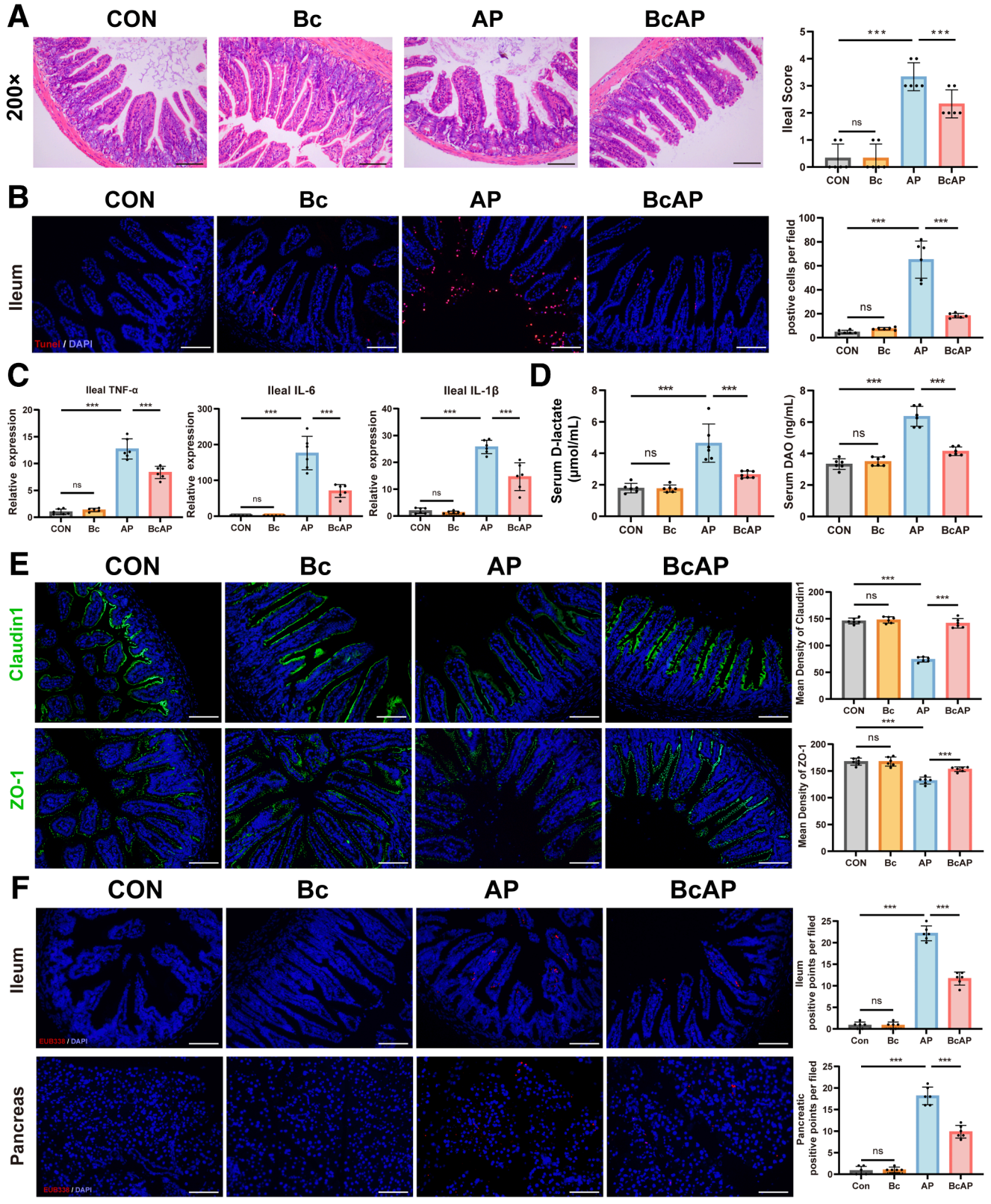
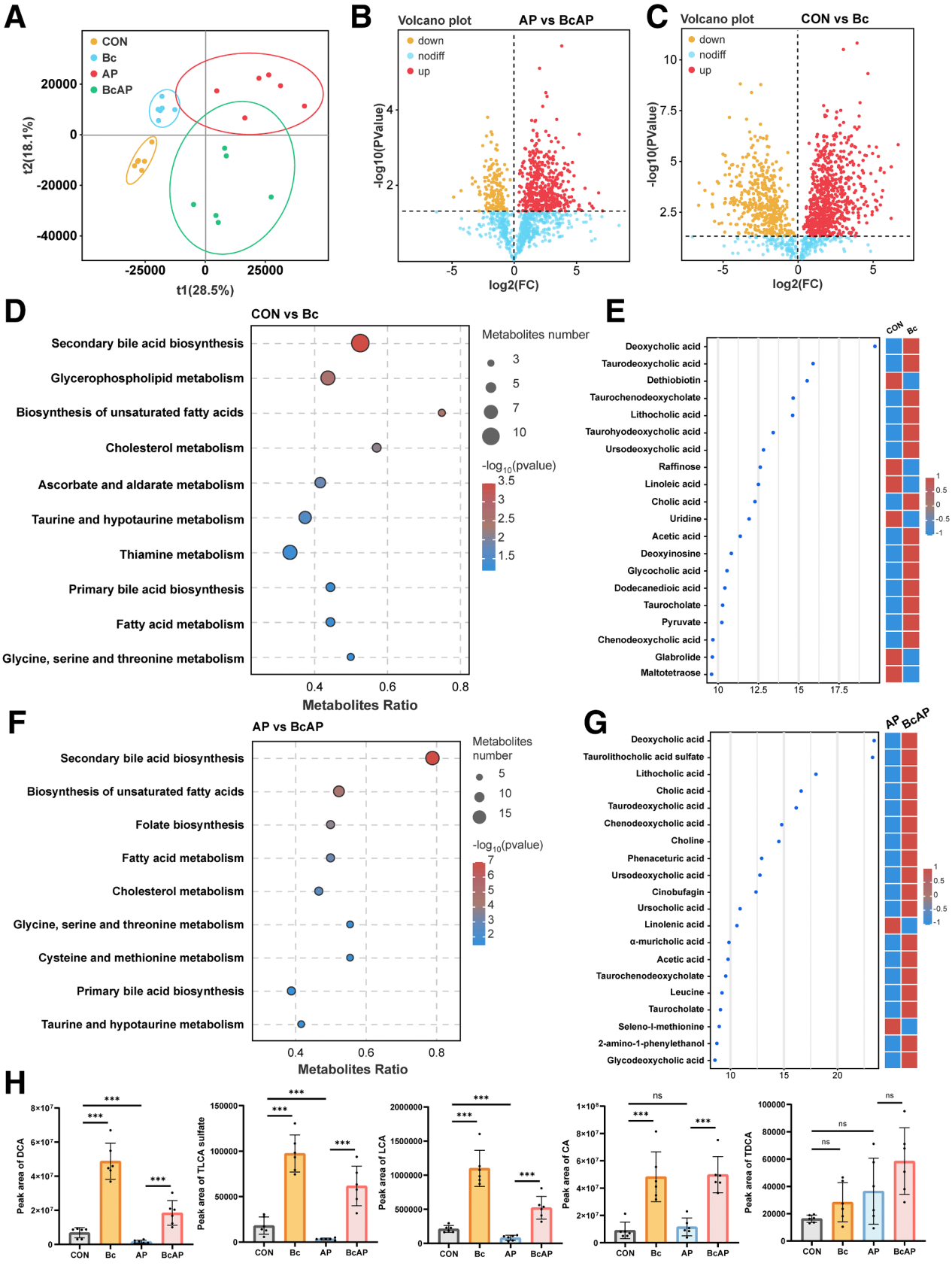


Figure 2. *B coccoides* mitigated ileal injuries in AP. (*A*) Histopathological changes and pathological scores of the ileum. Original magnification, ×200. (*B*) TUNEL staining and quantification of TUNEL+ cell in ileum. Original magnification, ×200. (*C*) Real-time PCR analysis of TNF-α, IL-6, IL-1β mRNA level in ileum; Tubulin was used as the reference gene. (*D*) Levels of serum D-lactate and DAO. (*E*) IF staining for Claudin1 and ZO-1 (*green*) in the ileum. Original magnification, ×100. (*F*) FISH tests of bacteria translocation in the ileum and pancreas by the EUB338 probe. Original magnification, ×200. The data are presented as the means ± SEM (n = 6 mice per group). **P* < .05; ***P* < .01; ****P* < .001. Bc, *Blautia coccoides*.


A
CON
Bc
AP
BcAP
t2(18.1%)
t1(28.5%)
B
Volcano plot
AP vs BcAP
down
nodiff
up
-log10(PValue)
log2(FC)
C
Volcano plot
CON vs Bc
down
nodiff
up
-log10(PValue)
log2(FC)
D
CON vs Bc
Secondary bile acid biosynthesis
Glycerophospholipid metabolism
Biosynthesis of unsaturated fatty acids
Cholesterol metabolism
Ascorbate and aldarate metabolism
Taurine and hypotaurine metabolism
Thiamine metabolism
Primary bile acid biosynthesis
Fatty acid metabolism
Glycine, serine and threonine metabolism
Metabolites Ratio
Metabolites number
-log10(pvalue)
E
Deoxycholic acid
Taurodeoxycholic acid
Dethiobiotin
Taurochenodeoxycholate
Lithocholic acid
Taurohyodeoxycholic acid
Ursodeoxycholic acid
Raffinose
Linoleic acid
Cholic acid
Uridine
Acetic acid
Deoxyinosine
Glycocholic acid
Dodecanedioic acid
Taurocholate
Pyruvate
Chenodeoxycholic acid
Glabrolide
Maltotetraose
CON
Bc
F
AP vs BcAP
Secondary bile acid biosynthesis
Biosynthesis of unsaturated fatty acids
Folate biosynthesis
Fatty acid metabolism
Cholesterol metabolism
Glycine, serine and threonine metabolism
Cysteine and methionine metabolism
Primary bile acid biosynthesis
Taurine and hypotaurine metabolism
Metabolites Ratio
Metabolites number
-log10(pvalue)
G
Deoxycholic acid
Taurolithocholic acid sulfate
Lithocholic acid
Cholic acid
Taurodeoxycholic acid
Chenodeoxycholic acid
Choline
Phenaceturic acid
Ursodeoxycholic acid
Cinobufagin
Ursocholic acid
Linolenic acid
α-muricholic acid
Acetic acid
Taurochenodeoxycholate
Leucine
Taurocholate
Seleno-l-methionine
2-amino-1-phenylethanol
Glycodeoxycholic acid
AP
BcAP
H
Peak area of DCA
Peak area of TLCA sulfate
Peak area of LCA
Peak area of CA
Peak area of TDCA
CON
Bc
AP
BcAP
ns

alleviate pancreatic and ileal histopathological damage in AP mice (Figure 7*B*–*F*), indicating that the protective effect requires live bacteria. Then, we found that *B coccoides*, which could ameliorate AP in our study, lacks the genes for BSH and the *bai* operon responsible for 7α-dehydroxylase via functional genomic annotation in Nr, Swiss-Prot, KEGG, and Clusters of Orthologous Genes/Groups (COG) databases (Figure 7*G*). Consistently, in contrast to the classical BSH-producing strain *Limosilactobacillus reuteri*, *B coccoides* failed to deconjugate bile acid amides, indicating a lack of BSH activity via ninhydrin assay (Figure 7*H*). Liquid chromatography-mass spectrometry (LC-MS) further confirmed that *B coccoides* could not convert chenodeoxycholic acid to DCA in vitro, demonstrating undetectable 7α-dehydroxylase activity (Figure 7*I*). These findings indicate that *B coccoides* does not promote DCA production through its own metabolism to influence AP.

Gut microbial metabolism is often driven by cooperative interactions among different species, where metabolites produced by one microbe can serve as substrates or signaling molecules for others. Therefore, we performed 16S rRNA sequencing to examine whether *B coccoides* intervention altered the abundance of bacteria known to possess BSH and 7α-dehydroxylase. AP induction led to a significant decrease in microbial alpha-diversity, which was restored by *B coccoides* gavage (Figure 8*A*). At the genus level, *B coccoides* supplementation significantly increased the relative abundance of BSH-producing genera, including *Parabacteroides* and *Bacteroide*, whereas the abundance of *Clostridium* and *Eubacterium*, known to possess 7α-dehydroxylase, are unchanged (Figure 8*B* and *C*). Antibiotic ablation in AP mice abolished the protective effects of *B coccoides* in alleviating pancreatic and intestinal injuries, whereas fecal microbiota transplantation from *B coccoides*-treated donors restored the phenotype, indicating that its therapeutic efficacy in AP is mediated through modulation of the gut microbiota (Figure 8*D*–*K*). In vitro co-culture experiments were performed to confirm bacterial interactions. The supernatant from *B coccoides* cultures significantly promoted the growth of *Parabacteroides* species (*P distasonis*, *P merdae*, *P johnsonii*) and *Bacteroides* species (*B uniformis*, *B thetaiotaomicron*, *B vulgatus*) species, whereas heat-inactivated bacteria and ultrasonically disrupted bacteria had no such effect (Figure 9*A* and *B*).

PICRUSt2 analysis of 16S rRNA data implied that, compared with CON mice, AP mice had a significant decreased abundance of BSH encoding gene, and BcAP mice exhibited an increased abundance (Figure 9*C*). The abundance of *bai* genes (*baiA, baiB, baiCD, baiE,* and *baiN*) encoding 7α-dehydroxylase did not differ between the AP and BcAP groups (Figure 9*C*). This prediction was subsequently validated by real-time PCR (Figure 9*D*). The conjugated BA hydrolysis assay (glycocholic acid, glycodeoxycholic acid and glycochenodeoxycholic acid) confirmed that fecal BSH enzyme activity was significantly elevated in the BcAP group (Figure 9*E* and *F*). Mantel test analysis revealed positive associations between BSH-producing bacteria (*Parabacteroides* and *Bacteroides*) and DCA (Figure 9*G*). *bsh* gene expression and *Blautia* abundance were also positively correlated with the relative abundance of these bacteria (Figure 9*H*). These findings suggest that *B coccoides* enhances SBAs production by enriching BSH-producing bacteria and upregulating microbial BSH activity.

We then administered BSH inhibitor along with *B coccoides* treatment in AP mice to link BSH activity to the protective effects of *B coccoides* (Figure 10*A*). BSH inhibition significantly diminished the ameliorative effects of *B coccoides* on pancreatic and ileal histopathological damage, serum amylase levels, and the expression of intestinal tight junction proteins in AP (Figure 10*B*–*G*). Targeted metabolomics confirmed that BSH inhibition reversed the *B coccoides*-induced modulation of bile acid profiles, leading to an increase in PBAs and a decrease in SBAs, such as DCA, lithocholic acid (LCA), and ursodeoxycholic acid (Figure 10*H*).

To determine if BSH activity of gut microbiota alone could attenuate AP, we engineered *Escherichia coli* BL21 to heterologously express a *bsh* gene from *Bifidobacterium adolescentis 1-11* (*E coli* BL21-BSH) (Figure 11*A*). The engineered strain exhibited high BSH activity in vitro (Figure 11*B*). Wild-type *E coli BL21* did not alter the severity of AP. Compared with those with wild-type *E coli BL21,* AP mice gavaged with *E coli* BL21-BSH presented significantly reduced pancreatic and ileal injury, lower serum amylase levels and inflammatory cytokine expression, and improved intestinal barrier protein expression (Figure 11*C*–*I*). Fecal SBAs via targeted metabolomics, such as DCA, LCA, and hyodeoxycholic acid, were significantly increased in *E coli* BL21-BSH+AP mice, as confirmed by targeted metabolomics (Figure 11*J*).

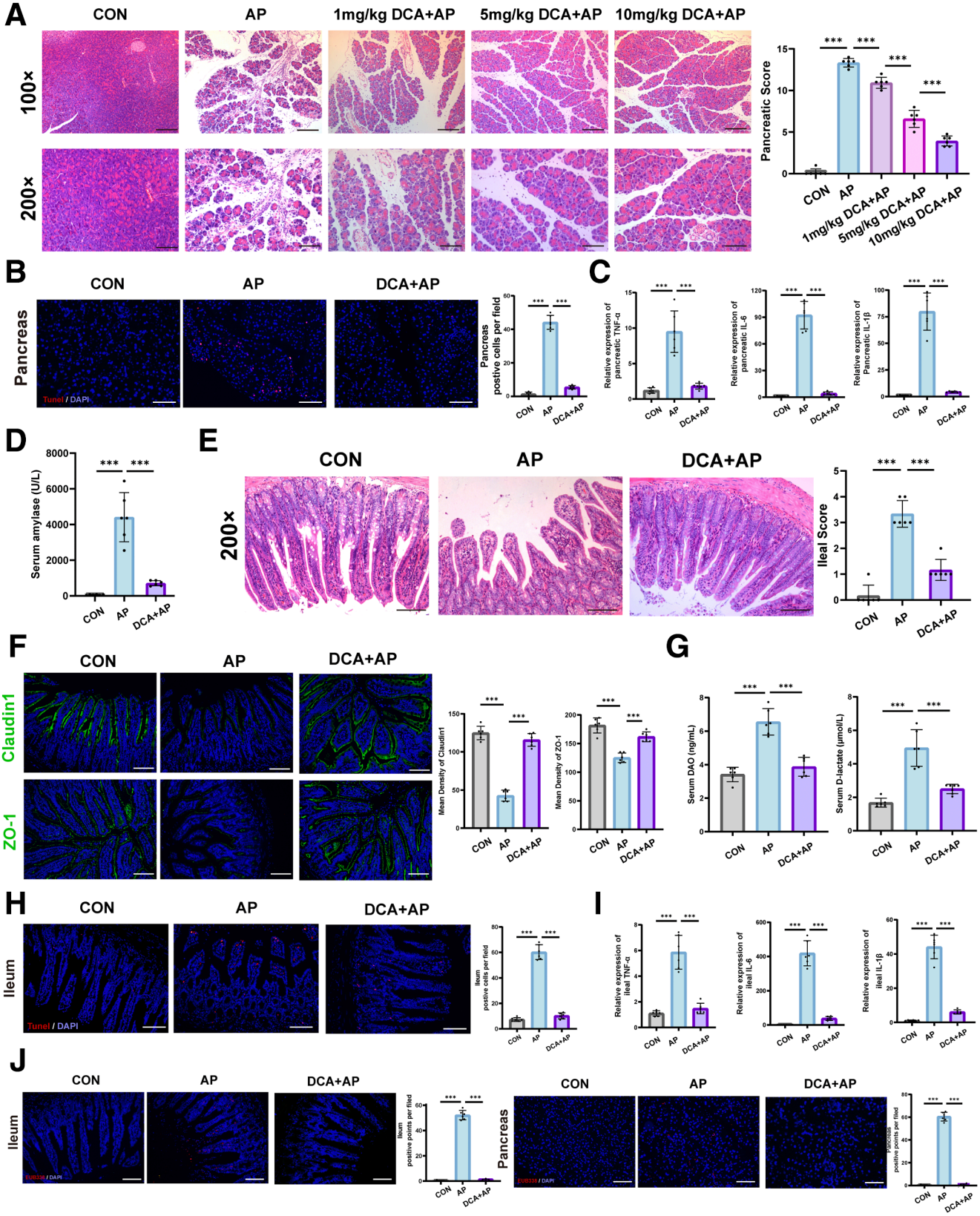
Collectively, these results confirmed that *B coccoides* exerts its therapeutic effects in AP though BSH-mediated BA metabolism.

A Combination of Bacterial Markers Showed Potential for Predicting the Severity of AP

Given our mechanistic findings, we analyzed the abundance of *B coccoides*-enriched genus (*Parabacteroides*,

Figure 3. (***See previous page***). ***B coccoides*** **regulated BA metabolism.** (*A*) PLS-DA analysis. (*B*) Volcano plot of significantly altered metabolites between AP group and BcAP group (Log2Fc $>$ 0). (*C*) Volcano plot of significantly altered metabolites between CON group and Bc group (Log2Fc $>$ 0). (*D*) KEGG enrichment analysis of differential metabolites between CON group and Bc group. (*E*) The VIP value plots of the differential metabolites (the top 20 of VIP value) metabolites between CON group and Bc group. (*F*) KEGG enrichment analysis of differential metabolites between AP group and BcAP group. (*G*) The VIP value plots of the differential metabolites (the top 20 of VIP value) metabolites between AP group and BcAP group. (*H*) Level of DCA, taurolithocholic acid sulfate, LCA, CA, taurodeoxycholic acid in feces. The data are presented as the means $\pm$ SEM (n = 6 mice per group). **P* $<$ .05; ***P* $<$ .01; ****P* $<$ .001.

Bacteroides) and the fecal *bsh* gene levels in patients with AP. Both *Parabacteroides* abundance and *bsh* gene levels decreased in a severity-dependent manner, being significantly lower in the SAP group than in the MAP/MSAP group, whereas *Bacteroides,* although reduced in AP, showed no difference between the MAP/MSAP and SAP



groups (Figure 12*A*–*C*). *Parabacteroides* abundance and fecal *bsh* gene abundance showed significant negative correlations with laboratory indicators (C-reactive protein [CRP], white blood cells [WBC]) and clinical severity scores (APACHE II, BISAP, PASS, Ranson scores), and *Bacteroides* abundance was negatively correlated with CRP, APACHE II, BISAP, and PASS scores (Figure 12*D*). Using receiver operating characteristic (ROC) curve analysis, a combined model incorporating the abundance of *Blautia*, *Parabacteroides*, *Bacteroides*, and *bsh* gene levels effectively distinguished patients with AP from HCs, achieving an area under the curve (AUC) of 97.3% (Figure 12*E*). This 4-marker panel also demonstrated strong predictive capability for identifying patients who would develop SAP, with an AUC of 90.5% (Figure 12*F*). When patients with AP were further stratified into hypertriglyceridemia AP and acute biliary pancreatitis, the model retained its predictive value for SAP with AUCs of 87.5% and 94.1%, respectively (Figure 12*G* and *H*).

Discussion

AP is a common gastrointestinal emergency with an increasing incidence in recent years. Gut dysbiosis is considered a critical factor in the pathogenesis of AP, yet the precise mechanisms remain to be elucidated. This study systematically unveils the protective role of *Blautia coccoides*. We observed that the abundance of *B coccoides* was negatively correlated with AP severity, and subsequently confirmed that supplementation with live *B coccoides* significantly ameliorated pancreatic and intestinal injury in experimental AP. Mechanistically, we found that *B coccoides* enhances BSH activity and BSH-producing bacteria *Bacteroides* and *Parabacteroides*, which restores the level of DCA and activates the FXR-FGF15 signaling pathway, effectively alleviating the progression of AP.

The genus *Blautia*, particularly *B coccoides*, as one of the core functional genera in the human gut, has recently garnered significant attention for its broad health-promoting potential as a "next-generation probiotic."[15] It is not only a major producer of SCFAs, but its diverse metabolic capabilities are also continuously being unveiled.[15] *B coccoides* and its metabolite acetate could also enhance the function of CD8+ T cells in a GPR43-dependent manner.[20] Furthermore, it maintains the normal function of the colonic mucus layer by secreting acetate and propionate to activate the FFAR2 receptor.[21] Studies have also shown that *B coccoides* can ameliorate metabolic disorders by producing indole-3-acetic acid,[22] or enhance the efficacy of bladder cancer immunotherapy by producing trigonelline.[23] We reveal that *B coccoides* alleviates experimental AP, which greatly expands its beneficial role.

Having established the protective role of *B coccoides*, our study further identified DCA as the key downstream effector molecule. Metabolomic analysis revealed DCA as a core metabolite that is significantly reduced during AP and restored following *B coccoides* treatment. The sufficiency of DCA was confirmed by exogenous supplementation experiments, where DCA gavage dose-dependently replicated the protective effects of *B coccoides* intervention. Although DCA may exhibit some cytotoxicity at supraphysiological concentrations,[24] growing evidence indicates that DCA is a crucial signaling molecule with broad beneficial roles in various pathophysiological processes. Its most prominent effects are immunomodulatory and anti-inflammatory. For instance, in a dextran sodium sulfate (DSS)-induced colitis model characterized by DCA deficiency due to dysbiosis, DCA supplementation significantly alleviated intestinal inflammation.[13] This anti-inflammatory capacity extends beyond the gut, as it also reduces the severity of experimental mastitis, inflammatory arthritis, and autoimmune uveitis.[25–27] Furthermore, DCA possesses anti-infective properties. Studies have confirmed that DCA can not only effectively inhibit the replication of the African swine fever virus (ASFV) but also be used to prevent and treat bacterial infections.[28,29] DCA also plays a positive role in tissue repair and regeneration. It can promote intestinal wound healing and crypt regeneration by inhibiting prostaglandin E2 (PGE2) production.[30] Concurrently, it can enhance angiogenesis by promoting the secretion of angiopoietin-like protein 4 (Angptl4).[31] Therefore, our finding that restoring intestinal DCA levels exerts a clear therapeutic benefit in AP is consistent with the broad consensus of DCA as a multi-potent and protective metabolite.

FXR is a high-affinity ligand for DCA. Previous studies have shown that activation of pancreatic FXR, using either obeticholic acid or adeno-associated virus, exerted direct protection on AP by restoring autophagic flux and mitochondrial function, whereas acinar-specific deletion of FXR exacerbated AP in mice.[8,32] Our study showed that oral gavage of DCA in AP mice markedly increased fecal DCA levels and intestinal FXR expression, whereas serum and pancreatic DCA levels and pancreatic FXR expression remained unchanged. We therefore concluded that DCA alleviated AP by activating intestinal FXR, which engages 2 canonical downstream pathways, including inhibiting

Figure 4. (***See previous page***). **DCA attenuated pancreatic and intestinal injuries in AP.** (*A*) Histopathological changes and pathological scores of the pancreas. Original magnification, ×100 (top panels) or ×200 (bottom panels). (*B*) TUNEL staining and quantification of TUNEL+ cell in pancreas. Original magnification, ×200. (*C*) Real-time PCR analysis of TNF-α, IL-6, IL-1β mRNA level in pancreas; Tubulin was used as the reference gene. (*D*) Serum amylase activity. (*E*) Histopathological changes and pathological scores of the ileum. Original magnification, ×200. (*F*) Immunofluorescence staining for Claudin1 and ZO-1 (*green*) in the ileum. Original magnification, ×100. (*G*) Levels of serum D-lactate and DAO. Original magnification, ×200. (*H*) TUNEL staining and quantification of TUNEL+ cell in ileum. Original magnification, ×200. (*I*) Real-time PCR analysis of TNF-α, IL-6, IL-1β mRNA level in ileum; Tubulin was used as the reference gene. (*J*) FISH tests of bacteria translocation in the ileum and pancreas by the EUB338 probe. The data are presented as the means ± SEM (n = 6 mice per group). *$P < .05$; **$P < .01$; ***$P < .001$.

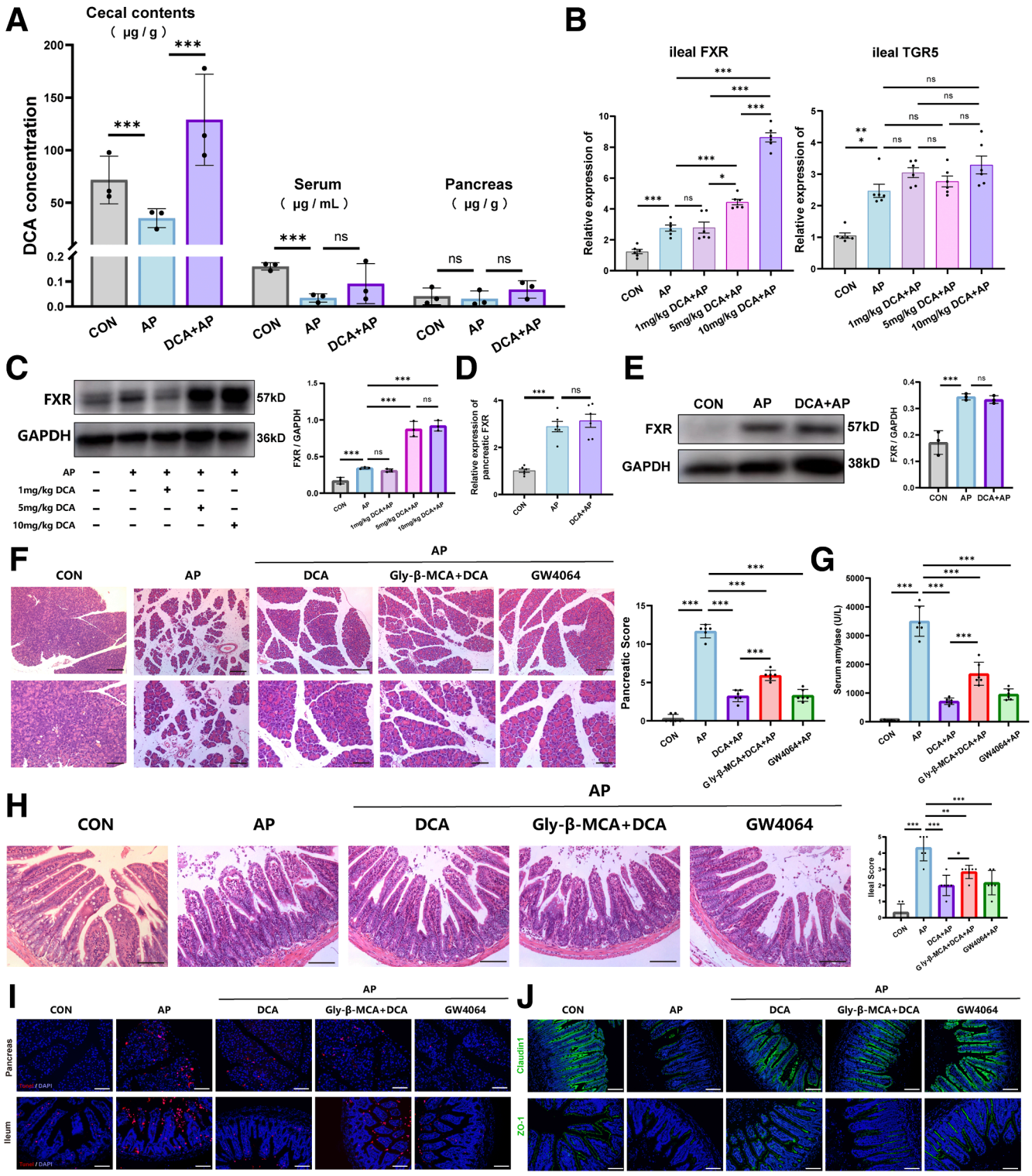
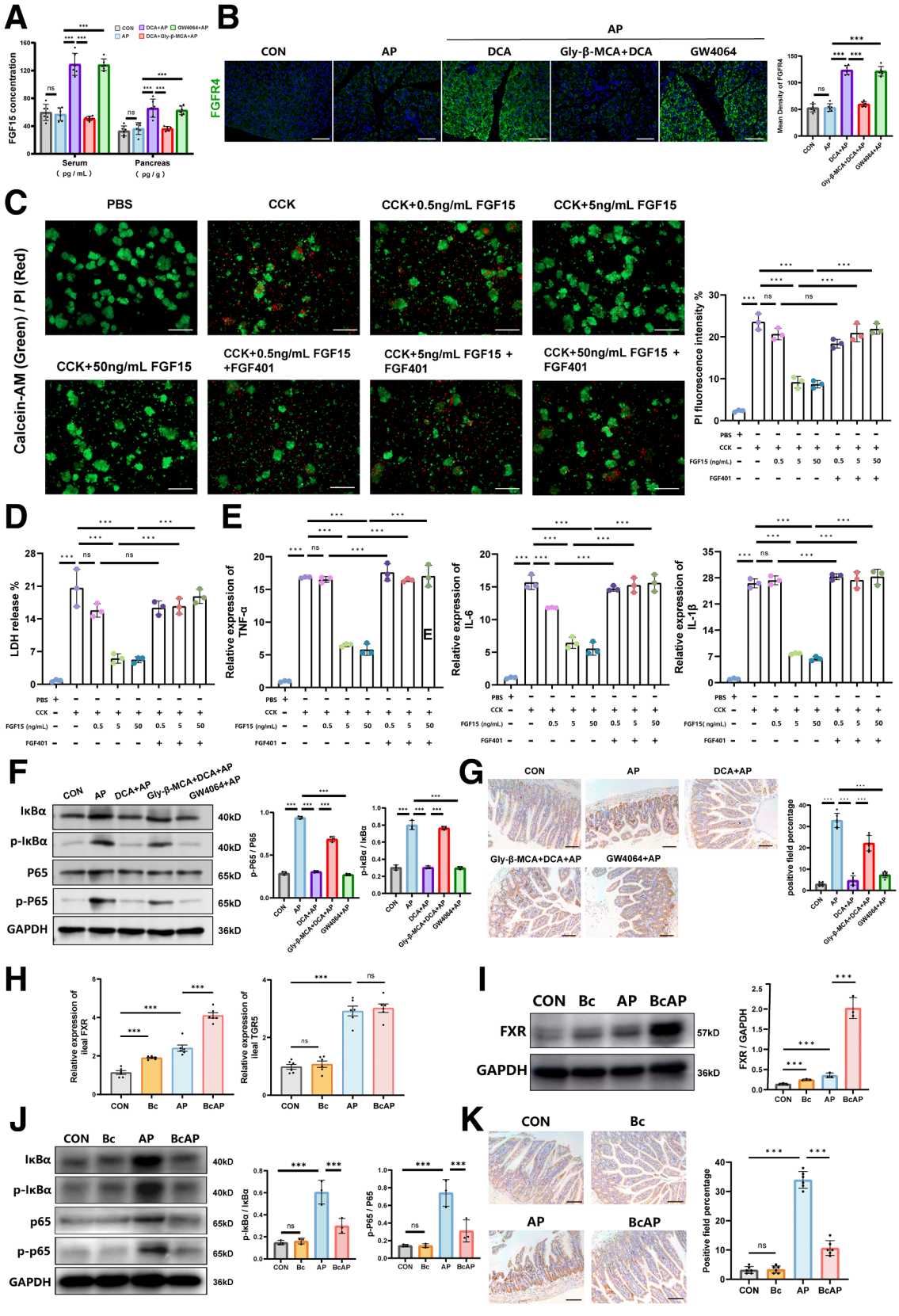


Figure 5. DCA mitigated AP in an FXR-dependent manner. (*A*) Alterations in cecal, pancreatic, and serum DCA levels (n = 3). (*B*) Real-time PCR analysis of ileal FXR and TGR5 mRNA levels; Tubulin was used as the reference gene. (*C*) Western blot analysis of ileal FXR. (*D*) Real-time PCR analysis of FXR mRNA level in pancreas; Tubulin was used as the reference gene. (*E*) Western blot analysis of pancreatic FXR. (*F*) Histopathological changes and pathological scores of the pancreas. Original magnification, ×100 (top panels) or ×200 (bottom panels). (*G*) Serum amylase activity. (*H*) Histopathological changes and pathological scores of the ileum. Original magnification, ×200. (*I*) TUNEL staining and quantification of TUNEL+ cell in pancreas and ileum. Original magnification, ×200. (*J*) IF staining for Claudin1 and ZO-1 (*green*) in the ileum. Original magnification, ×100. The data are presented as the means ± SEM (n = 3 or 6 mice per group). **P* < .05; ***P* < .01; ****P* < .001.

phosphorylation of NF-κB and NLRP3 inflammasome and activating the transcription of FGF15. Our data showed that DCA suppressed ileal NF-κB/NLRP3 signaling, and increased pancreatic FGF15 in AP mice. It has been demonstrated that restoring FGF15 levels by activating intestinal FXR can effectively protect the liver injury in



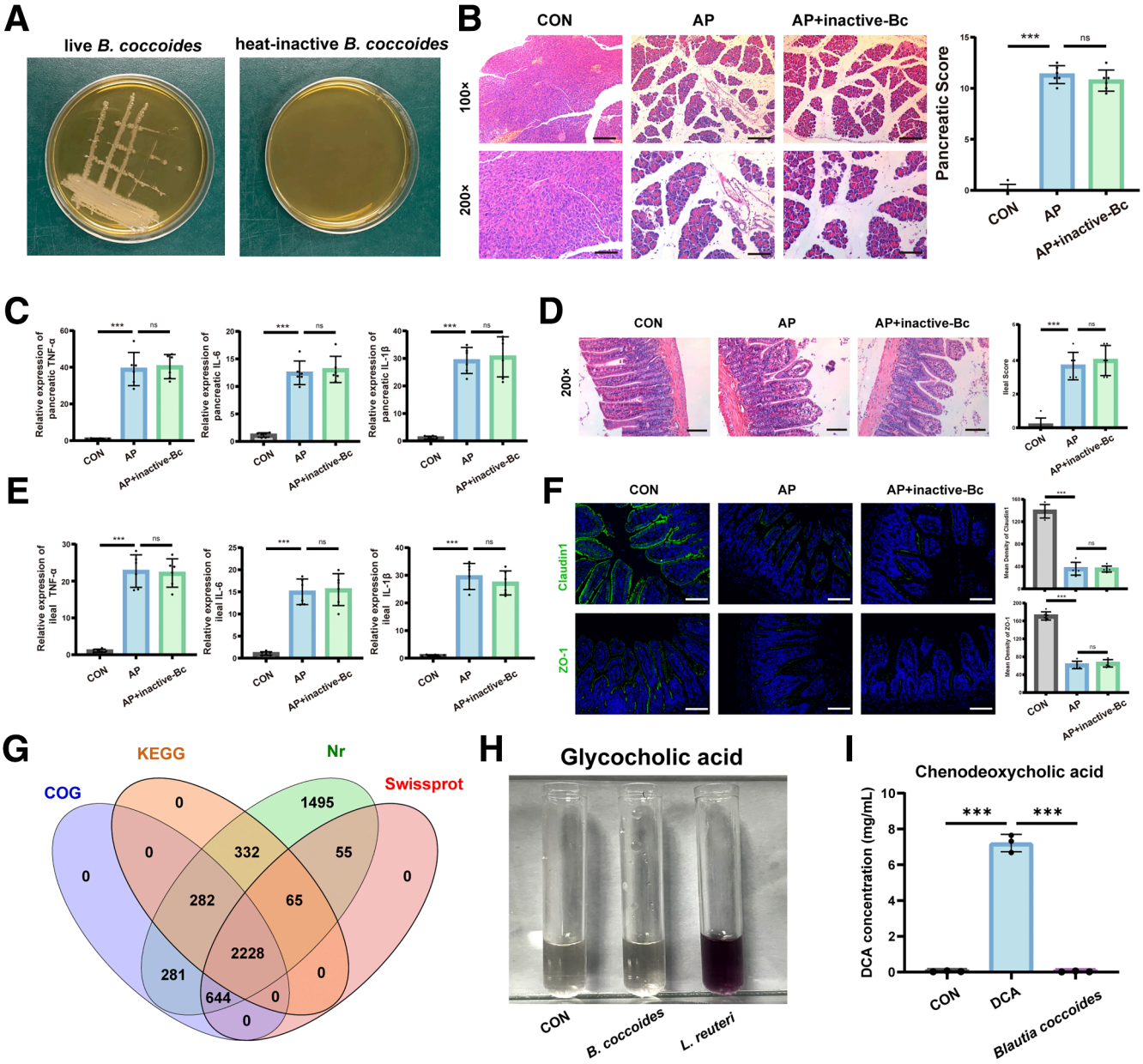
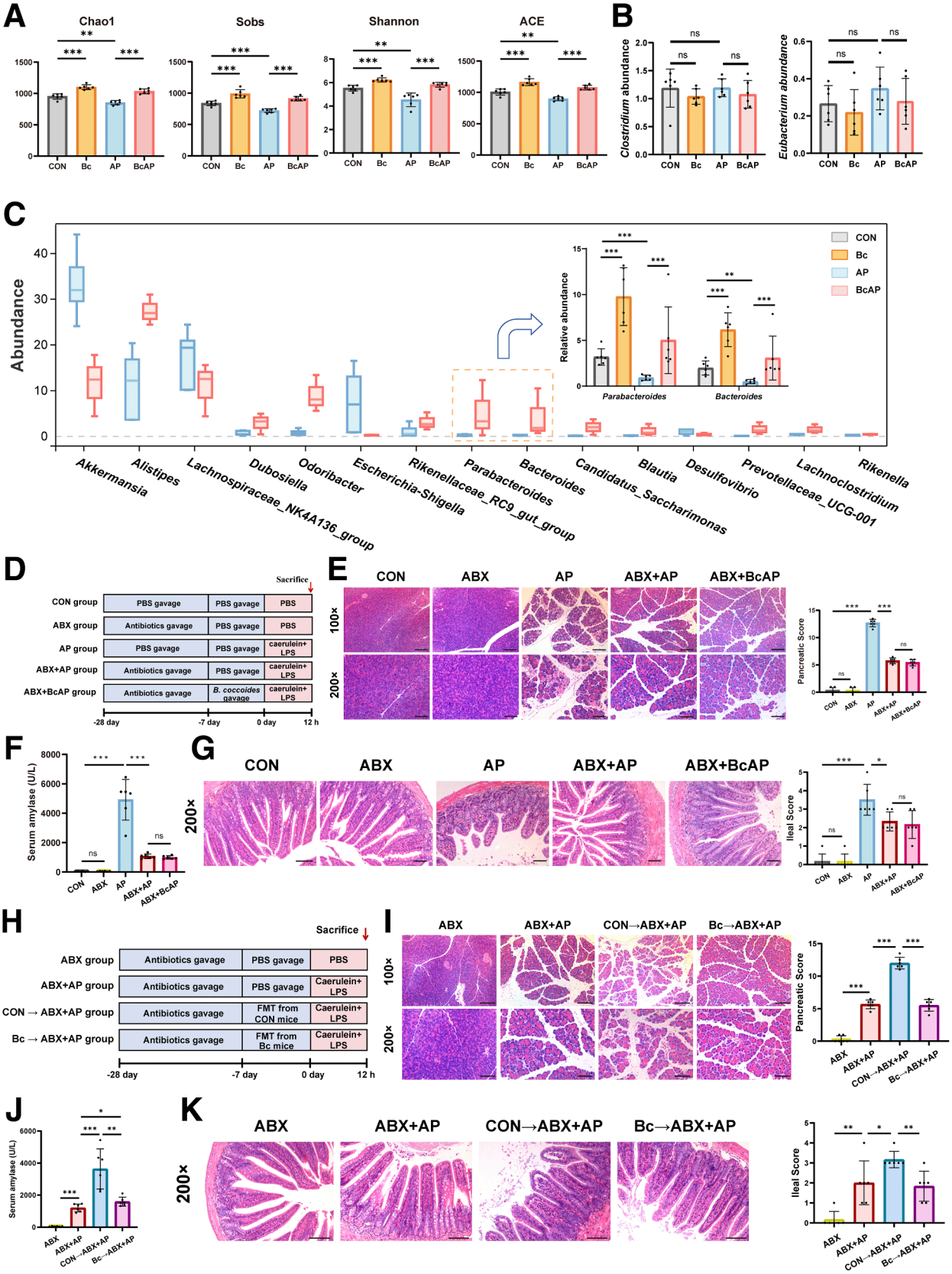


Figure 7. Heat-inactivated *B coccoides* failed to alleviate AP. (*A*) Plate spreading of *B coccoides*. (*B*) Histopathological changes and pathological scores of the pancreas. Original magnification, ×100 (*top panels*) or ×200 (*bottom panels*). (*C*) Real-time PCR analysis of TNF-α, IL-6, IL-1β mRNA level in pancreas; Tubulin was used as the reference gene. (*D*) Histopathological changes and pathological scores of the ileum. Original magnification, ×200. (*E*) Real-time PCR analysis of TNF-α, IL-6, IL-1β mRNA level in ileum; Tubulin was used as the reference gene. (*F*) IF staining for Claudin1 and ZO-1 (*green*) in the ileum. Original magnification, ×100. (*G*) Venn diagram of annotations from 4 major databases. (*H*) Ninhydrin assay (substrate: glycocholic acid). (*I*) DCA concentration in the culture supernatant (substrate: chenodeoxycholic acid) by targeted metabolomics. The data are presented as the means ± SEM (n = 6 mice per group). **P* < .05; ***P* < .01; ****P* < .001. Bc, *Blautia coccoides;* nr, non-redundant protein database.

Figure 6. (***See previous page***). **DCA protected acinar cells by activating pancreatic FGF15 signaling.** (*A*) Levels of FGF15 in the serum and pancreas. (*B*) IF staining for FGFR4 in the ileum. Original magnification, ×200. (*C*) Assessment of cell viability by Calcein-AM (*green*)/PI (*red*) staining. (*D*) LDH cytotoxicity assay to assess cell death. (*E*) Real-time PCR analysis of TNF-α, IL-1β, IL-6 mRNA level in acinar cells; Tubulin was used as the reference gene. (*F*) Western blot analysis of ileal p-IκBα/IκBα, p-p65/p65. (*G*) IHC analysis of NLRP3 expression in the ileum. (*H*) Real-time PCR analysis of pancreatic FXR and TGR5 mRNA levels; Tubulin was used as the reference gene. (*I*) Western blot analysis of ileal FXR. (*J*) Western blot analysis of ileal IκBα/p-IκBα, p65/p-p65. (*K*) IHC analysis of NLRP3 expression in the ileum. The data are presented as the means ± SEM (n = 6 mice per group). **P* < .05; ***P* < .01; ****P* < .001.

alcoholic liver disease.[33] Similarly, dysregulation of the intestinal FXR-FGF15 signal is closely linked to lipid metabolism disorders in diet-induced dyslipidemia.[34] Our findings confirmed that recombinant FGF15 reduced acinar injury in vitro. Thus, modulating the intestinal FXR-FGF15 pathway could be a therapeutic strategy for AP.



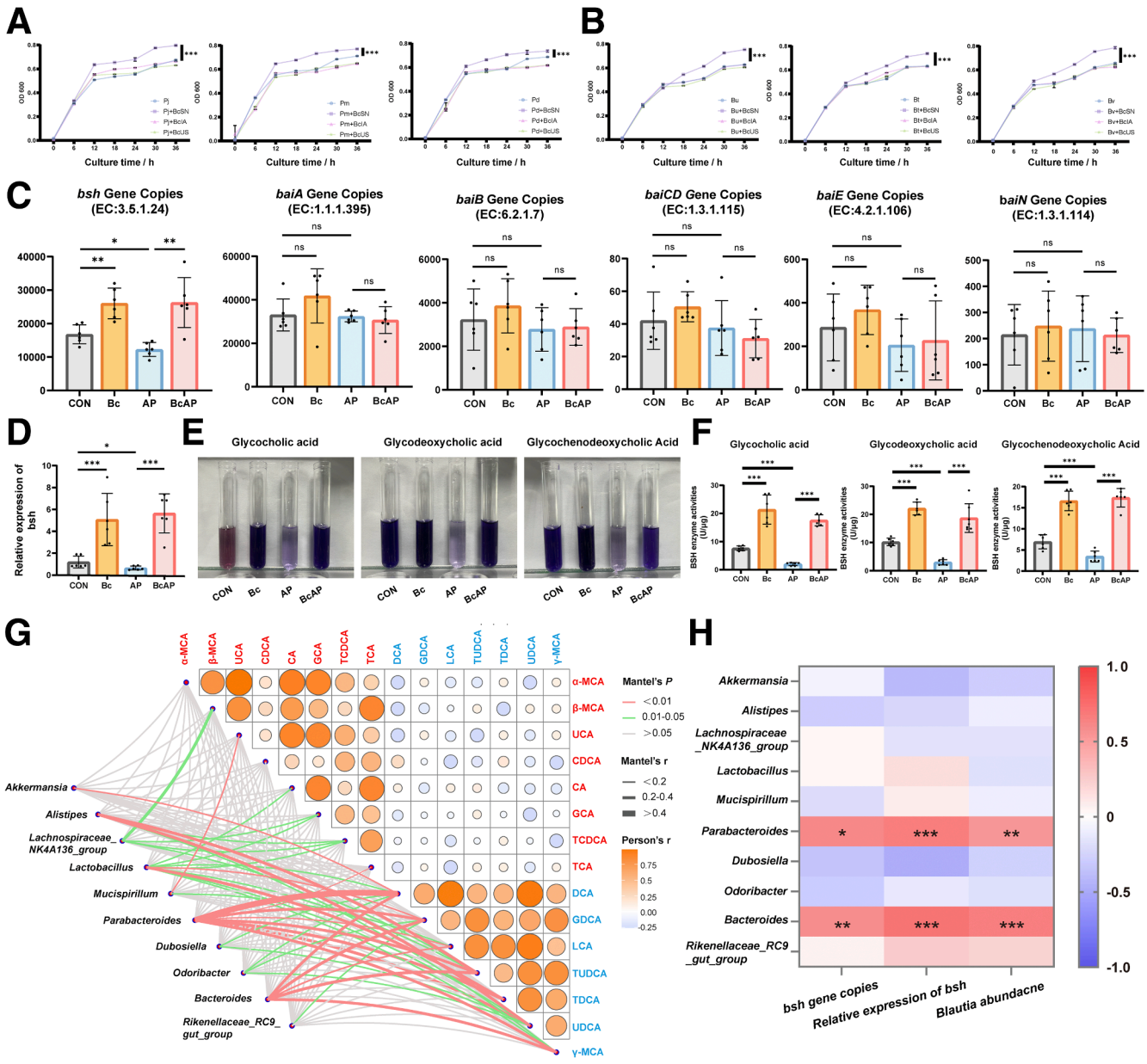


Figure 9. Activity of fecal BSH and abundance of BSH producing bacteria were elevated by *B coccoides*. (*A*) Growth curves of representative strains (Pj, Pm, Pd) of the genus *Parabacteroides* over 36 hours. (*B*) Growth curves of representative strains (Bu, Bt, Bv) of the genus *Bacteroides* over 36 hours. (*C*) PICRUSt2 analysis of *bsh* and different *bai* genes genes copy numbers. (*D*) Relative quantification of the *bsh* gene in mouse feces. (*E*) Ninhydrin assay. (*F*) Fecal BSH enzyme activity in each mouse group. (*G*) Mantel test analysis of the correlation between the top 10 most abundant genera and the fecal BA metabolic profile. (*H*) Heatmap of the Spearman correlation between the abundance of the top 10 genera and the copy number and relative expression of the *bsh* gene. The data are presented as the means ± SEM (n = 6 mice per group). **P* < .05; ***P* < .01; ****P* < .001. Bt, *Bacteroides thetaiotaomicron*; Bu, *Bacteroides uniformis*; Bv, *Bacteroides vulgatus*; IA, inactivation; Pd, *Parabacteroides distasonis*; Pj, *Parabacteroides johnsonii*; Pm, *Parabacteroides merdae*; SN, supernatant; US, ultrasound.

Figure 8. (***See previous page***). ***B coccoides* attenuated AP in a gut microbiota-dependent manner.** (*A*) Alpha diversity (Chao1 index, Sobs index, Shannon index, Ace index) of gut microbiota. (*B*) Relative abundance of *Clostridium* and *Eubacterium*. (*C*) The bar graph of the relative abundance of the top 15 genera in cecum between AP and BcAP group. (*D*) Schematic of the experimental procedure. (*E*) Histopathological changes and pathological scores of the pancreas. Original magnification, ×100 (top panels) or ×200 (bottom panels). (*F*) Serum amylase activity. (*G*) Histopathological changes and pathological scores of the ileum. Original magnification, ×200. (*H*) Schematic of the experimental procedure. (*I*) Histopathological changes and pathological scores of the pancreas. Original magnification, ×100 (top panels) or ×200 (bottom panels). (*J*) Serum amylase activity. (*K*) Histopathological changes and pathological scores of the ileum. Original magnification, ×200. The data are presented as the means ± SEM (n = 6 mice per group). **P* < .05; ***P* < .01; ****P* < .001. ABX, antibiotics cocktail; Bc, *Blautia coccoides*.

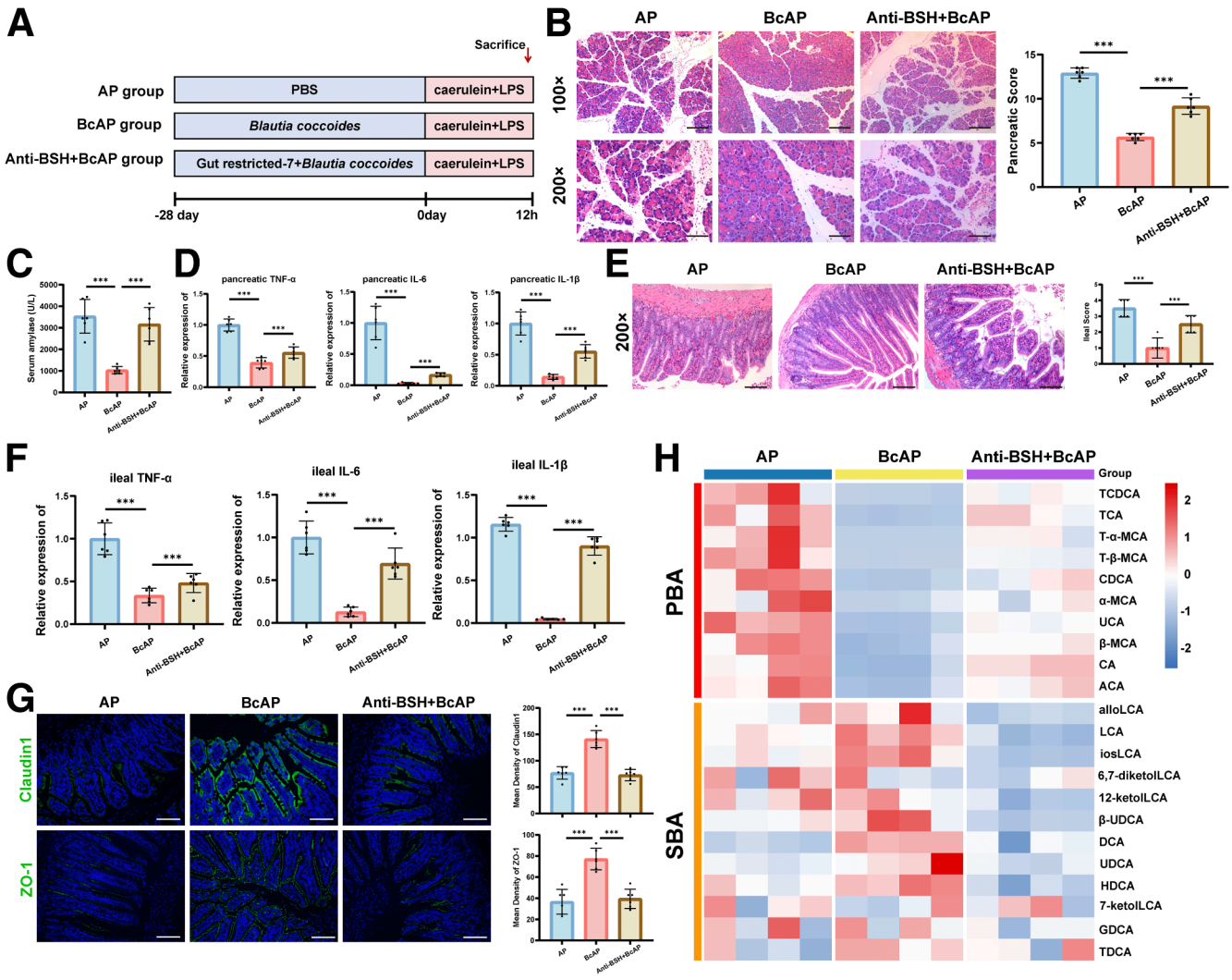


Figure 10. Inhibition of BSH activity reduced the protective role of *B coccoides* in AP. (*A*) Schematic of the experimental procedure. (*B*) Histopathological changes and pathological scores of the pancreas. Original magnification, ×100 (top panels) or ×200 (bottom panels). (*C*) Serum amylase activity. (*D*) Real-time PCR analysis of TNF-α, IL-6, IL-1β mRNA level in pancreas; Tubulin was used as the reference gene. (*E*) Histopathological changes and pathological scores of the ileum. Original magnification, ×200. (*F*) Real-time PCR analysis of TNF-α, IL-6, IL-1β mRNA level in ileum; Tubulin was used as the reference gene. (*G*) IF staining for Claudin1and ZO-1 (*green*) in the ileum. Original magnification, ×100. (*H*) Heatmap of targeted BA metabolism. The data are presented as the means ± SEM (n = 6 mice per group). **P* < .05; ***P* < .01; ****P* < .001.

Our results clearly indicate that the therapeutic effect of *B coccoides* requires live, metabolically active bacteria. This finding raises a central question: how does *B coccoides* regulate DCA levels? The generation of SBAs is a 2-step process. BSH hydrolyzes conjugated PBAs into unconjugated PBAs, which is often considered rate-limiting. Subsequently, the 7α-dehydroxylase encoded by bai genes utilizes these unconjugated PBAs to produce SBAs, such as DCA.[12] Our results demonstrated that *B coccoides* significantly increased both the *bsh* gene abundance and BSH enzyme activity in the gut microbiota of AP mice, whereas the abundance of *bai* genes showed no significant change. Studies have shown that BSH inhibitors such as AAA-10 could lower fecal DCA and LCA,[35] whereas upregulating BSH or administering probiotics with BSH activity such as *Lactobacillus reuteri* increased fecal DCA.[36,37] In this study, BSH inhibitor Gut-restricted 7 (GR-7) abolished the therapeutic effects of *B coccoides* and reduced fecal DCA levels, whereas oral gavage of engineered *E coli* expressing BSH could alleviate AP and markedly elevated fecal DCA levels. In summary, the increase in fecal DCA after *B coccoides* gavage is attributable to enhanced BSH activity, thereby increasing the availability of free PBAs.

Our in vitro co-culture experiments further revealed that the culture supernatant of *B coccoides* can significantly promote the growth of *Parabacteroides* and *Bacteroides* species, which possess high BSH activity. This represents a more complex and indirect mode of probiotic action. Although the specific secreted factors mediating this interaction remain to be identified, we propose several plausible mechanisms based on existing literature. First, *B coccoides* produces metabolites including acetate, lactate,

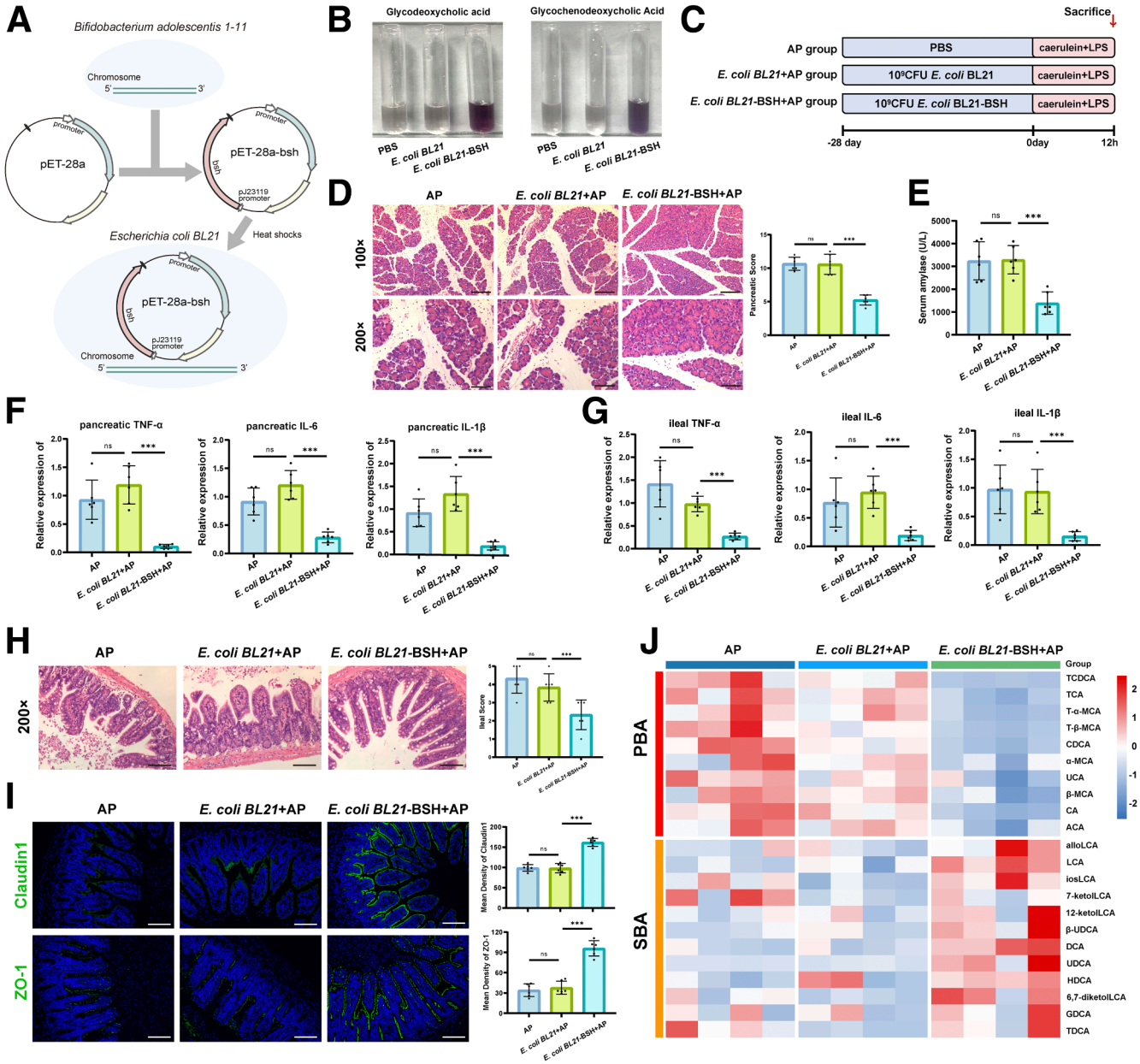


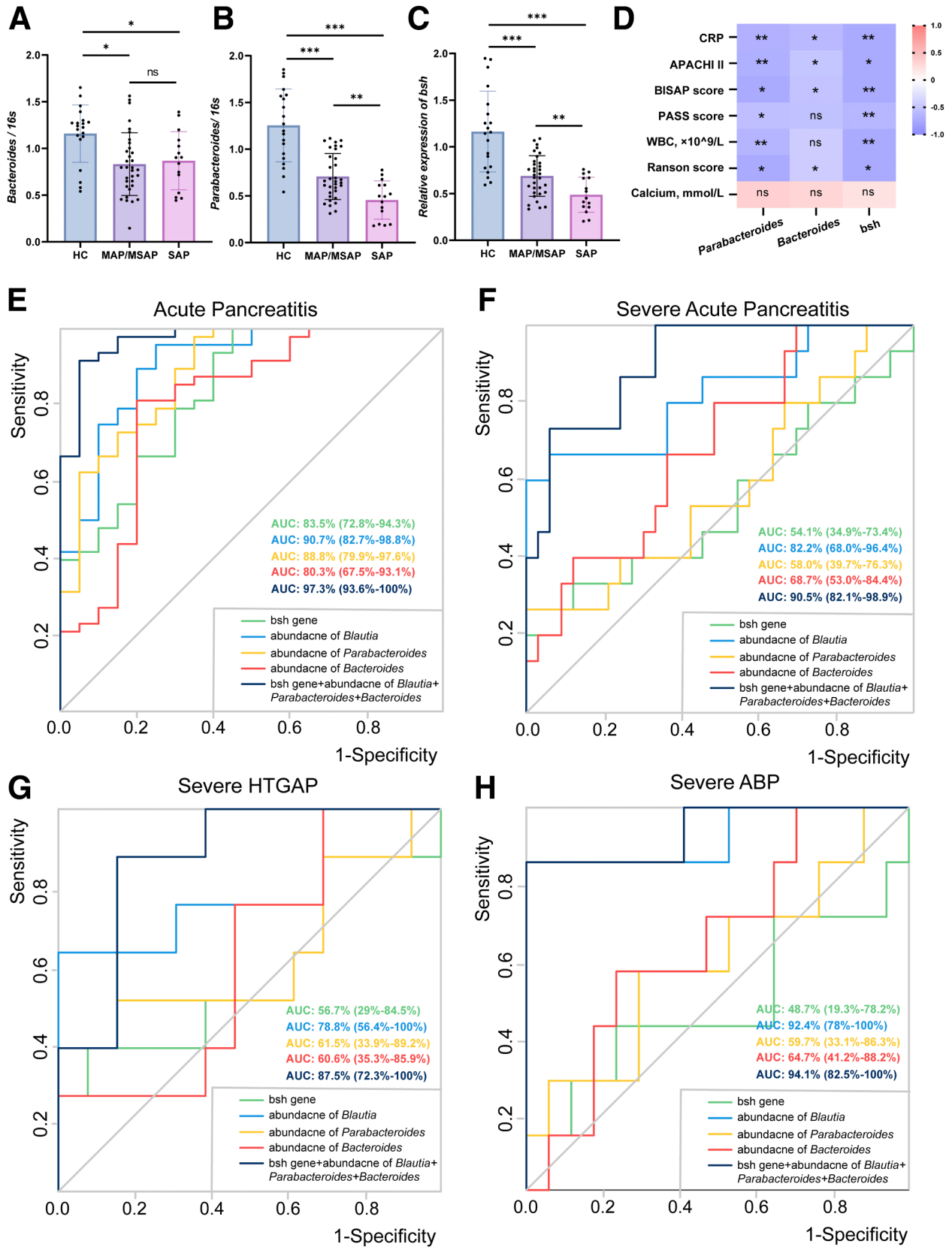
Figure 11. BSH activity was critical for *B coccoides*–mediated protection against AP. (*A*) Schematic diagram illustrating the construction of *E coli* for the heterologous expression of *bsh*. (*B*) Detection of BSH activity using a ninhydrin colorimetric assay. (*C*) Schematic of the experimental procedure. (*D*) Histopathological changes and pathological scores of the pancreas. Original magnification, ×100 (top panels) or ×200 (bottom panels). (*E*) Serum amylase activity. (*F*) Real-time PCR analysis of TNF-α, IL-6, IL-1β mRNA level in pancreas; Tubulin was used as the reference gene. (*G*) Real-time PCR analysis of TNF-α, IL-6, IL-1β mRNA level in ileum; Tubulin was used as the reference gene. (*H*) Histopathological changes and pathological scores of the ileum. Original magnification, ×200. (*I*) Immunofluorescence staining for Claudin1and ZO-1 (*green*) in the ileum. Original magnification, ×100. (*J*) Heatmap of targeted BA metabolism. The data are presented as the means ± SEM (n = 6 mice per group). *$P < .05$; **$P < .01$; ***$P < .001$.

and succinate.[15] These SCFAs and organic acids could serve as energy sources or fermentation substrates for *Bacteroides* and *Parabacteroides*. Second, the metabolic activity of *B coccoides* may alter gut microenvironment, for instance by lowering pH, which is more favorable for the growth of BSH-producing bacteria.[38]

Some limitations exist in our study. The specific secreted factors mediating the interaction between *B coccoides* and BSH-producing bacteria remain to be identified. Our clinical data are correlational, and prospective human intervention studies are needed to establish causality. Future research should include translational

validation and therapeutic development, for instance, by using safe chassis microorganisms to express high-efficiency BSH enzymes for safer therapeutic delivery.

In conclusion, this study provides demonstration of how a single gut commensal, *B coccoides*, combats AP by regulating a complex protective cascade. These findings position



B coccoides, BSH, and DCA as promising therapeutic targets for AP and offer a valuable framework for exploring how gut microbes can be leveraged to influence AP.

Materials and Methods

Subjects and Sample Collection

The study was approved by the Ethics Committee of Shanghai General Hospital (2023078). All enrolled patients provided written informed consent to participate. Participants consented in writing to the publication of fully anonymized data. No identifying personal information is included in this article. An exploratory cohort of patients with AP was assembled to assess fecal *Blautia* alterations. Forty-eight individuals met the revised Atlanta diagnostic criteria for AP and were classified into 2 groups: 33 with MAP/MSAP and 15 with SAP.[39] Stool specimens were collected within 72 hours of AP onset. Twenty HCs undergoing routine health examinations served as controls. The baseline characteristic profiles (age, sex, and BMI) are shown in Table 1. Participants were excluded if they had chronic pancreatitis, inflammatory bowel disease, irritable bowel syndrome, gastrointestinal malignancy, celiac disease, fatty liver disease, type 2 diabetes, or if they had taken antibiotics, probiotics, or laxatives in the preceding 3 months, factors known to affect the gut microbiome. All fecal samples were immediately frozen at −80°C until analysis.

Animals and Experimental Design

All animal experiment protocols were approved by Institutional Animal Care and Use Committee (IACUC) of Shanghai General Hospital (2024AW033) and conducted according to the instructions of IACUC. Specific pathogen-free (SPF)-grade male C57BL/6J mice, aged 6 to 8 weeks (weighing 20–22 g), were obtained from Shanghai SLAC Company. All experimental animals were housed in the animal experiment center of Shanghai General Hospital under SPF conditions. The environment was maintained with a stable and moderate temperature, sufficient air exchange, appropriate humidity, and minimal noise. A 12-hour light/dark cycle was provided using incandescent lighting.

To investigate the potential protective role of *B coccoides* in AP, C57BL/6 mice received oral gavage of *B coccoides* at 10^8 colony forming units (CFU)/mL, followed by AP induction. Mice were assigned to CON, Bc, AP, and BcAP groups (n = 6). The AP model was established by intraperitoneal injection of 100 mg/kg cerulein (MedChemExpress) once hourly for 10 doses, with 5 mg/kg LPS (Sigma-Aldrich) administered together with the final injection. After AP induction, mice were euthanized, and the pancreas, serum, colon and cecal contents were collected and stored at −80°C or fixed in 4 % paraformaldehyde. To determine whether the protection conferred by *B coccoides* was attributable to metabolic activity rather than structural components, a heat-inactivated (pasteurized) preparation was generated by treatment at 70°C for 30 minutes and administered by gavage for 28 days prior to AP induction; all other procedures were identical.

To assess the impact of the markedly altered DCA on AP, C57BL/6 mice were gavaged with DCA (Sigma-Aldrich) at 1, 5, or 10 mg/kg daily for 1 week and then subjected to AP induction to evaluate dose-dependent effects on AP severity. Mice were randomized into CON, AP, 1 mg/kg DCA+AP, 5 mg/kg DCA+AP, and 10 mg/kg DCA+AP groups (n = 6).

To determine whether the therapeutic effect of *B coccoides* is mediated via the gut microbiota, we performed fecal microbiota transplantation (FMT). First, intestinal microbiota was depleted by oral gavage (200 μL/mouse/day) of an antibiotic cocktail (0.5 mg/mL vancomycin, 1 mg/mL neomycin, 1 mg/mL ampicillin, and 1 mg/mL metronidazole [Sangon]) for 28 days. Fresh feces from CON or Bc donor mice were prepared as a 100 mg/mL suspension. Antibiotic-pretreated recipients were randomized into ABX, ABX+AP, CON → ABX+AP, and Bc → ABX+AP groups (n = 6), received 200 μL fecal suspension by gavage daily for 7 days, and were then subjected to AP induction.

To establish the central role of BSH activity in *B coccoides*–mediated protection, we co-administered the BSH inhibitor GR-7 (10 mg/kg in corn oil containing 5% DMSO) (MedChemExpress) together with *B coccoides* by daily gavage for 28 days. Mice were assigned to AP, BcAP, and anti-BSH BcAP groups (n = 6). In addition, to test whether BSH activity alone is sufficient to ameliorate AP, we engineered *Escherichia coli* BL21 to express a *bsh* gene (*E coli* BL21-BSH). Mice were allocated to AP, *E coli* BL21+AP, and *E coli* BL21-BSH+AP groups (n = 6), received daily gavage for 28 days, and were then subjected to AP induction.

To elucidate downstream intestinal signaling of DCA, particularly the role of FXR, C57BL/6 mice were randomly assigned to 5 groups (n = 6 each): CON, AP, DCA+AP, Gly-β-MCA+DCA+AP, and GW4064+AP. Mice in the GW4064+AP group received the FXR agonist GW4064 (50 mg/kg) (MedChemExpress) to mimic the protective effect

Figure 12. (***See previous page***). **A gut microbiota-based biomarker panel for the diagnosis and severity prediction of AP.** (*A*) Levels of *Bacteroides* in feces of patients with AP with different severities. (*B*) Levels of *Parabacteroides* in feces of patients with AP with different severities. (*C*) Levels of the *bsh* gene in feces of AP patients with different severities. (*D*) Correlation between the relative abundance of *Parabacteroides*, *Bacteroides*, *bsh* gene and clinical indicators of patients with AP. (*E*) ROC curves for models predicting the presence of AP. (*F*) ROC curves for models predicting the progression to SAP. (*G*) ROC curves for models predicting the progression to severe HTGAP. (*H*) ROC curves for models predicting the progression to severe ABP. The data are presented as the means ± SEM (n = 6 mice per group). **P* < .05; ***P* < .01; ****P* < .001. ABP, acute biliary pancreatitis; HTGAP, hypertriglyceridemic acute pancreatitis.

of DCA during AP induction, whereas mice in the Gly-β-MCA+DCA+AP group received the intestinal FXR antagonist Gly-β-MCA (10 mg/kg) (MedChemExpress) together with DCA to assess FXR dependence.

Bacterial Strains and Culture

B coccoides DSM935, *Limosilactobacillus reuteri* ATCC23272, *Parabacteroides johnsonii* CCUG 54943T, *Parabacteroides merdae* JCM9497, *Parabacteroides distasonis* BNCC354946, *Bacteroides uniformis* ATCC8492, *Bacteroides thetaiotaomicron* DSM2079, and *Bacteroides vulgatus* ATCC8482 were obtained from BeNa Culture Collection. *B coccoides, P johnsonii, P merdae, P distasonis, B uniformis, B thetaiotaomicron*, and *B vulgatus* were grown in brain heart infusion (BHI) medium (237500; Becton, Dickinson) at 37°C for 36 to 48 hours in an anaerobic workstation (COY Vinyl Anaerobic Chambers). *B coccoides* collection was performed in an anaerobic workstation (4500 × g, 4°C, 10 minutes) and was washed twice with phosphate-buffered saline (PBS) buffer, resuspended and adjusted to a concentration of 10^8 CFU/mL. *L reuteri* were grown in DeMan, Rogosa, and Sharpe (MRS) medium (HB0384-5; Hope Bio).

Histological Examination

Following a 48-hour fixation in 4% paraformaldehyde at 4°C, both pancreatic and ileal tissues were processed for histological analysis. The procedure involved sequential washes with double-distilled water, a standard series of rehydration and dehydration steps, and subsequent embedding in paraffin. From these paraffin blocks, 4-μm sections were cut and mounted on slides for hematoxylin and eosin (H&E) staining. A light microscope (Leica) was used to examine the slides at 100× and 200× magnification. The Schmidt criteria were applied to assess pancreatic histopathology, and Chiu's method was used to evaluate damage to the ileum.

Real-time PCR

For gene expression analysis, total RNA was isolated from tissues using a tissue RNA purification kit plus (EZBioscience) and subsequently reverse-transcribed into cDNA with HyperScript III RT SuperMix (EnzyArtisan). In parallel, bacterial DNA was extracted from fecal samples using an E.Z.N.A. stool DNA kit (Omega). The concentration of all nucleic acids was determined using a NanoDrop2000 spectrophotometer (Thermo Scientific). Real-time PCR was then conducted on a QuantStudio 6 Flex system (Thermo Scientific) with the S6 universal SYBR qPCR mix (EnzyArtisan), and relative gene expression was calculated using the $2^{-\Delta\Delta Ct}$ method. Primers used are shown in Table 2.

Table 2. The Sequences of the Primers Used

Name	Sequences (5′-3′)
Mouse TNF-α	(F) CCTGTAGCCCACGTCGTAG
	(R) GGGAGTAGACAAGGTACAACCC
Mouse IL-6	(F) TACCACTTCACAAGTCGGAGGC
	(R) CTGCAAGTGCATCATCGTTGTTC
Mouse IL-1β	(F) GAAATGCCACCTTTTGACAGTG
	(R) TGGATGCTCTCATCAGGACAG
Mouse Tubulin	(F) GGCAGTGTTCGTAGACCTGGAA
	(R) CTCCTTGCCAATGGTGTAGTGG
16s	(F) GGTTACCTTGTTACGACTT
	(R) AGAGTTTGATCCTGGCTCAG
Blautia obeum	(F) GCGATCAGATTACGATCACTC
	(R) GCCATGCCAACACCTTTTTC
Blautia coccoides	(F) CGGTACCTGACTAAGAAGC
	(R) AGTTTCATTCTTGCGAACG
Blautia wexlerae	(F) GCATAAGCGCACAGAGCT
	(R) CACATCAGACTTGCCACA
Blautia producta	(F) AACTCCGGTGGTATCAGATG
	(R) GGGGCTTCTGAGTCAGGTA
Blautia	(F) AAAGGCATGGGCTCAACCT
	(R) CCCTCCGGCACTCAAGTATG

Construction of BSH-expressing E coli Strain

The expression of BSH in *E coli* was conducted following previously described methods.[40] Briefly, the *bsh* gene from *Bifidobacterium adolescens* 1-11 and the pJ23119 promoter were incorporated into the pET-28a plasmid via gene synthesis. This resulting pET-28a-*bsh* plasmid was then introduced into *E coli* BL21 cells using a heat shock method (42°C for 90 seconds). Following a 1-hour incubation in Lysogeny broth (LB) broth, the transformed cells were plated on LB agar medium containing ampicillin and incubated at 37°C.

16S rRNA Sequencing

Cecal contents were collected and immediately stored at −80°C until processing. Total microbial genomic DNA was isolated from the samples using the HiPure Stool DNA Kit (Magen) according to the manufacturer's protocol. The V3–V4 hypervariable region of the 16S rRNA gene was amplified from the extracted DNA using the universal primers 341F (5′-CCTACGGGNGGCWGCAG-3′) and 806R (5′-GGACTACHVGGGTATCTAAT-3′). The quality of the PCR products was confirmed by 2% agarose gel electrophoresis. Amplicons were then purified using AMPure XP magnetic beads (Beckman Coulter) to remove primer-dimers and other contaminants. Sequencing libraries were subsequently prepared with the Illumina DNA Prep Kit (Illumina) as the manufacturer's guidelines. Qualified libraries were pooled and sequenced on the Novaseq 6000 platform using the PE250 mode. For the bioinformatic analysis, raw sequencing reads were first subjected to quality control using FASTP to remove adapters and low-quality sequences. The resulting clean reads were then merged into consensus tags using FLASH, requiring a minimum overlap of 12 bp and allowing a maximum mismatch rate of 2%. The QIIME 2 DADA2 pipeline was employed to denoise the sequences, remove primers, and resolve amplicon sequence

variants (ASVs). After chimera removal, a feature table containing the final, non-chimeric ASV sequences and their corresponding abundances was generated. Taxonomic classification of the ASVs was performed by aligning against the SILVA reference database. All subsequent bioinformatic analyses were conducted using the Omicsmart online data analysis platform (http://www.omicsmart.com). The 16s rRNA sequencing data are available into the National Center for Biotechnology Information (NCBI) Sequence Read Archive database at https://www.ncbi.nlm.nih.gov/bioproject/PRJNA1307155 with BioProject ID PRJNA1307155.

Enzyme-linked Immunosorbent Assay

Serum levels of diamine oxidase (BPE20139), D-lactate (BPE20072) and fibroblast growth factor 15 (EK1113) were quantified using enzyme-linked immunosorbent assay (ELISA) kits from MultiSciences Biotech, following the manufacturers' protocols.

Serum Amylase Assay

Serum amylase levels were measured on an Advia 2400 automated chemistry analyzer (Siemens) using the instrument's enzymatic assay protocol supplied by the manufacturer.

Preparation of FMT

Fresh feces from CON or Bc donor mice were collected into sterile tubes containing pre-cooled PBS and processed within 30 minutes. Samples were adjusted to 100 mg/mL, vigorously vortexed for 5 minutes. The supernatant was filtered through a sterile 70-μm nylon cell strainer into sterile tubes. Filtrates were kept on ice and administered within 1 hour of preparation.

Western Blot

Ileal tissues were lysed in RIPA buffer (Epizyme Biotech) containing a protease inhibitor (Epizyme Biotech). After centrifugation, supernatants were mixed with sodium dodecyl sulfate (SDS)-loading buffer (Epizyme Biotech) and heated. Protein samples (10 μL) were separated by 7.5% SDS-polyacrylamide gel electrophoresis (PAGE) using a PAGE gel kit (PG111, Epizyme Biotech) and transferred to 0.2 μm polyvinylidene fluoride (PVDF) membranes (Millipore). The membranes were blocked for 1 hour with 3% bovine serum albumin (BSA), then incubated overnight at 4°C with primary antibodies against p65 (A19653; Abclonal), phospho-p65 (AP1294; Abclonal), IκBα (A19714; Abclonal), phospho-IκBα (AP0707; Abclonal), and FXR (A24015; Abclonal) diluted in primary antibody dilution buffer (Epizyme Biotech). Following washes with Tris-buffered saline with Tween 20 (TBST), membranes were probed for 1 hour with horseradish peroxidase (HRP)-conjugated goat anti-rabbit IgG(H+L) (Epizyme Biotech). Finally, bands were visualized using an HRP substrate peroxide solution (Millipore) on an Amersham 600 imager (General Electric).

Immunofluorescence and Immunohistochemistry

For immunofluorescence (IF) analysis, ileal tissue sections were first heated at 60°C for 1 hour, followed by deparaffinization and rehydration using a Leica Autostainer XL (Leica). Antigen retrieval was subsequently performed in a citrate solution (Sangon Biotech). After washing with PBS, the sections were outlined with a super pap pen (Biosharp) and then treated with immunostaining blocking buffer (Sangon Biotech, China) for 1 hour at room temperature. Following the blocking step, tissues were incubated overnight at 4°C with primary antibodies targeting claudin1 (ab211737; Abcam, USA), ZO-1 (13663; Cell Signaling Technology), or FGFR4 (11098-1-AP; Proteintech) prepared in primary antibody dilution buffer (Sangon Biotech). The next day, slides were washed with PBS, incubated for 1 hour at room temperature with Alexa Fluor 488/594 AffiniPure donkey anti-rabbit IgG (Yeason), and washed again. Finally, nuclei were counterstained with 4′,6-diamidino-2-phenylindole (DAPI; Yeason) for 10 minutes, and images were acquired using a fluorescence microscope (Leica).

For immunohistochemistry (IHC) staining, tissue sections underwent the same deparaffinization, rehydration, antigen retrieval, and blocking procedures described above. The sections were then incubated overnight at 4°C with a primary antibody against NLRP3 (68102-1-Ig; Proteintech). Following primary antibody incubation, detection was carried out using an HRP-polymer IHC kit (G1215; Servicebio) according to the manufacturer's protocol. The signal was visualized with a diaminobenzidine (DAB) substrate, and the sections were subsequently counterstained with hematoxylin. After dehydration and mounting, the slides were imaged using a light microscope.

Terminal Deoxynucleotidyl Transferase dUTP Nick-end Labeling and FISH Assays

Apoptosis in pancreatic and ileal tissues was assessed using a terminal deoxynucleotidyl transferase dUTP nick-end labeling (TUNEL) Apoptosis Assay Kit (Red Fluorescence) (Beyotime) following the manufacturer's protocol. To detect bacterial translocation via FISH, sections of the same tissues were first dewaxed, underwent antigen retrieval, and were then digested with proteinase K for 5 minutes at 37°C. Subsequently, the sections were pre-hybridized for 1 hour at 37°C, followed by overnight hybridization at 37°C in a humidified chamber with the EUB338 probe (5'-Cy3-GCTGCCTCCCGTAGGAGT-3'). After post-hybridization washes, the sections were counterstained with DAPI, and images were acquired with a fluorescence microscope (Leica).

Untargeted Metabolomics

Metabolite extraction was performed on 100 mg of each sample. Samples were first homogenized in 1 mL of ice-cold 90% methanol using an MP homogenizer (2 cycles at 6.0 M/S for 60s each). The resulting homogenates were then subjected to 2 cycles of low-temperature sonication for 30

minutes each to ensure complete cell lysis. After sonication, the mixture was centrifuged at 14,000 g for 20 minutes at 4°C. The supernatant was carefully collected and dried completely in a vacuum centrifuge. For analysis, the dried metabolite pellet was reconstituted in 100 μL of a 50% acetonitrile/water (v/v) solution. Samples were analyzed using an ultra-high-performance liquid chromatography (UHPLC) system (1290 Infinity LC) coupled to a quadrupole time-of-flight mass spectrometer (TripleTOF 6600). Chromatographic separation was performed using a hydrophilic interaction liquid chromatography (HILIC) method on an ACQUITY UPLC BEH Amide column (2.1 mm × 100 mm, 1.7 μm) (Waters). The mobile phase consisted of Solvent A (25 mM ammonium acetate and 25 mM ammonium hydroxide in water and Solvent B (acetonitrile). The elution gradient was programmed as follows: maintained at 95% B for 0.5 minutes, linearly decreased to 65% B over 6.5 minutes, reduced to 40% B over 1 minute and held for 1 minute, then returned to 95% B in 0.1 minute, followed by a 3-minute re-equilibration period. The mass spectrometer was operated in both positive and negative electrospray ionization (ESI) modes. The ESI source conditions were set as follows: source temperature, 600°C; IonSpray Voltage Floating, ±5500 V; Ion Source Gas 1, 60 psi; Ion Source Gas 2, 60 psi; and curtain gas, 30 psi. Data were acquired in information-dependent acquisition mode with high sensitivity. Full scan time of flight mass spectometry (TOF-MS) data was acquired over an m/z range of 60 to1000 Da with an accumulation time of 0.20 seconds. For MS/MS acquisition, product ion scans were acquired over an m/z range of 25 to 1000 Da with an accumulation time of 0.05 seconds. Up to 10 candidate ions per cycle were selected for fragmentation, with a fixed collision energy of 35 V (±15 eV) and a declustering potential of ±60 V. Isotope exclusion was set at 4 Da. Bioinformatic analysis was performed using Omicsmart, a real-time interactive online platform for data analysis (http://www.omicsmart.com).

Calcein/Propidium Iodide Cell Viability/Cytotoxicity Assay

Cell viability was assessed using a Calcein-AM/propidium iodide (PI) kit (C1371; Beyotime, China). Primary pancreatic acinar cells were washed with PBS and incubated with the 1× working solution at 37°C for 10 minutes in the dark. Fluorescence was imaged by fluorescence microscopy. Live/dead proportions were calculated after background subtraction. All other steps followed the manufacturer's protocol.

Lactate Dehydrogenase Cytotoxicity Assay

Cytotoxicity was quantified using a lactate dehydrogenase (LDH) kit (C0018; Beyotime). Cell-free supernatants were transferred to a 96-well plate and mixed with the LDH working reagent according to the manufacturer's instructions. After incubation at room temperature for 10 to 30 minutes in the dark, stop solution was added, and absorbance was read at 450 nm. Each assay included untreated control wells, Total LDH wells (complete lysis), and no-cell background wells (same medium). Absorbance values were background-corrected by subtracting no-cell readings.

Targeted Metabolomics

For targeted analysis of BAs, samples were subjected to a methanol-based extraction. Briefly, 600 μL of ice-cold methanol was added to each sample, followed by vortexing for 60 seconds. Insoluble debris was pelleted by centrifugation at 12,000 rpm for 10 minutes at 4°C. A 400-μL aliquot of the resulting supernatant was transferred to a new tube and dried completely using a vacuum concentrator. The dried extract was then reconstituted in 100 μL of a 30% methanol solution. Prior to analysis, the reconstituted sample was clarified by filtration through a 0.22-μm membrane, and the filtrate was transferred to an autosampler vial. Chromatographic separation was achieved using an ACQUITY UPLC BEH C18 column (Waters) maintained at 40°C. An injection volume of 5 μL was used for all analyses. The mobile phase consisted of 0.01% formic acid in water (Solvent A) and acetonitrile (Solvent B), delivered at a flow rate of 0.25 mL/min. The gradient elution program was as follows: 25% B from 0 to 4 minutes; 25% to 30% B from 4 to 9 minutes; 30% to 36% B from 9 to 14 minutes; 36% to 38% B from 14 to 18 minutes; 38% to 50% B from 18 to 24 minutes; 50% to 75% B from 24 to 32 minutes; 75% to 90% B from 32 to 33 minutes; and returning to 25% B from 33 to 35.5 minutes. The UPLC system was coupled to a mass spectrometer equipped with an ESI source operating in negative ion mode. Key ion source parameters were set as follows: temperature, 500°C; ion spray voltage, −4500 V; curtain gas, 30 psi; nebulizer gas, 50 psi; and turbo gas, 50 psi. Quantification was performed in multiple reaction monitoring mode.

BSH Activity Assay

Total fecal BSH activity was quantified by measuring the release of free amino acids from conjugated bile salt substrates using a ninhydrin-based colorimetric assay.[40,41] Fresh fecal samples from mice were homogenized in PBS and passed through a 40-μm cell strainer. The filtrate was centrifuged at 10,000 g for 10 minutes at 4°C to pellet the bacterial cells. The cell pellet was washed and resuspended in 0.1 M sodium phosphate buffer (pH 6.5). The bacterial suspension was then subjected to ultrasonication on ice (300 W, 5 seconds on, 5 seconds off, for a total of 30 minutes). The resulting lysate was clarified by centrifugation at 10,000 g for 10 minutes at 4°C, and the supernatant, containing the crude enzyme extract, was collected for the activity assay. A similar procedure was used to prepare crude enzyme extract from cultured *B coccoides* after adjusting the bacterial culture to an OD_{600} of 1.0.

The reaction mixture consisted of 100 μL of crude enzyme extract, 1.8 mL of 0.1 M sodium phosphate buffer (pH 6.5), and 100 μL of a 6 mM conjugated bile salt substrate solution (glycocholate, glycodeoxycholate, or glycochenodeoxycholate). The mixture was incubated at 37°C for 30 minutes. The reaction was terminated by adding 100 μL of 15% (w/v) trichloroacetic acid. After centrifugation to

remove precipitates, 200 μL of the supernatant was mixed with 1.0 mL of distilled water and 1.0 mL of ninhydrin reagent. The mixture was heated in a boiling water bath for 30 minutes, cooled to room temperature, and the absorbance was measured at 570 nm. The amount of released amino acid was quantified using a standard curve generated with known concentrations of glycine. One unit of BSH activity was defined as the amount of enzyme required to release 1 μmol of amino acid from the substrate per minute.

Isolation of Primary Pancreatic Acinar Cells and Intervention

Primary pancreatic acinar cells (PACs) were isolated from mice using a collagenase-based dissociation procedure.[42] Briefly, pancreatic tissues were excised into ice-cold PBS, gently rinsed, and injected at multiple sites with 1 mL 2 mg/mL collagenase IV solution (HY-E70005D; MedChemExpress). Tissues were incubated at 37°C for 20 minutes, then mechanically dispersed with wide-bore pipette tips until small acinar clusters predominated. The suspension was passed through a 70-μm cell strainer (Corning), centrifuged, washed, and resuspended in Dulbecco's Modified Eagle Medium (DMEM)/F-12 supplemented with 10% fetal bovine serum (FBS). PACs were then pre-incubated with recombinant FGF15 (0.5, 5, or 50 ng/mL) and the FGFR4 inhibitor FGF-401 (10 μM) for 6 hours, followed by stimulation with 1 mM CCK octapeptide (HY-P0196; MedChemExpress). Cells were then collected for downstream analyses as described in the figure legends.

Statistical Methods

The variables of continuous data with normal distribution are expressed as standard error of the mean (SEM) and the variables with non-normal distribution were expressed as median (interquartile range [IQR]). Comparisons between 2 groups with a normal distribution were performed by *t*-test. Mann-Whitney *U* test was used for the comparisons between 2 groups with non-normal distribution. Single-factor analysis of variance (ANOVA) was used for comparison among 3 or more groups. For categorical variables, data were expressed as numbers and percentages and evaluated by χ^2 test. Spearman's rank correlation coefficient was used to determine correlations. All the statistical analyses were carried out in IBM SPSS Statistics 25. $P < .05$ indicates that the difference was statistically significant.

References

1. Lee PJ, Papachristou GI. New insights into acute pancreatitis. Nat Rev Gastroenterol Hepatol 2019;16:479–496.
2. van Dijk SM, Hallensleben NDL, van Santvoort HC, et al. Acute pancreatitis: recent advances through randomised trials. Gut 2017;66:2024–2032.
3. Liu Q, Ruan K, An Z, et al. Updated review of research on the role of the gut microbiota and microbiota-derived metabolites in acute pancreatitis progression and inflammation-targeted therapy. Int J Biol Sci 2025;21:1242–1258.
4. Wang Z, Liu J, Li F, et al. The gut-lung axis in severe acute Pancreatitis-associated lung injury: the protection by the gut microbiota through short-chain fatty acids. Pharmacol Res 2022;182:106321.
5. Yan X, Li J, Wu D. The role of short-chain fatty acids in acute pancreatitis. Molecules 2023;28:4985.
6. Liu Q, Gu X, Liu X, et al. Long-chain fatty acids - the turning point between 'mild' and 'severe' acute pancreatitis. Heliyon 2024;10:e31296.
7. Wang D, Sun S, Zhao Q, et al. Metabolic shifts in tryptophan pathways during acute pancreatitis infections. JCI Insight 2025;10:e186745.
8. Zhu Q, Yuan C, Dong X, et al. Bile acid metabolomics identifies chenodeoxycholic acid as a therapeutic agent for pancreatic necrosis. Cell Rep Med 2023;4:101304.
9. Zhang X, Xin G, Li S, et al. Dehydrocholic acid ameliorates sodium taurocholate-induced acute biliary pancreatitis in mice. Biol Pharm Bull 2020;43:985–993.
10. Malo A, Krüger B, Seyhun E, et al. Tauroursodeoxycholic acid reduces endoplasmic reticulum stress, trypsin activation, and acinar cell apoptosis while increasing secretion in rat pancreatic acini. Am J Physiol Gastrointest Liver Physiol 2010;299:G877–G886.
11. Collins SL, Stine JG, Bisanz JE, et al. Bile acids and the gut microbiota: metabolic interactions and impacts on disease. Nat Rev Microbiol 2023;21:236–247.
12. Song Z, Cai Y, Lao X, et al. Taxonomic profiling and populational patterns of bacterial bile salt hydrolase (BSH) genes based on worldwide human gut microbiome. Microbiome 2019;7:9.
13. Sinha SR, Haileselassie Y, Nguyen LP, et al. Dysbiosis-induced secondary bile acid deficiency promotes intestinal inflammation. Cell Host Microbe 2020;27:659–670.e5.
14. Fu Y, Mei Q, Yin N, et al. Paneth cells protect against acute pancreatitis via modulating gut microbiota dysbiosis. mSystems 2022;7:e0150721.
15. Liu X, Mao B, Gu J, et al. Blautia-a new functional genus with potential probiotic properties? Gut Microbes 2021;13:1–21.
16. Zhang C, Li G, Lu T, et al. The interaction of microbiome and pancreas in acute pancreatitis. Biomolecules 2023;14:59.
17. Wahlström A, Sayin SI, Marschall HU, et al. Intestinal crosstalk between bile acids and microbiota and its impact on host metabolism. Cell Metab 2016;24:41–50.
18. Fuchs CD, Trauner M. Role of bile acids and their receptors in gastrointestinal and hepatic pathophysiology. Nat Rev Gastroenterol Hepatol 2022;19:432–450.
19. Hao H, Cao L, Jiang C, et al. Farnesoid X receptor regulation of the NLRP3 inflammasome underlies cholestasis-associated sepsis. Cell Metab 2017;25:856–867.e5.
20. Qiu J, Shi C, Zhang Y, et al. Microbiota-derived acetate is associated with functionally optimal virus-specific CD8(+) T cell responses to influenza virus infection via GPR43-dependent metabolic reprogramming. Gut Microbes 2024;16:2401649.

21. Holmberg SM, Feeney RH, Prasoodanan PKV, et al. The gut commensal Blautia maintains colonic mucus function under low-fiber consumption through secretion of short-chain fatty acids. Nat Commun 2024;15:3502.
22. Niu Y, Hu X, Song Y, et al. Blautia coccoides is a newly identified bacterium increased by leucine deprivation and has a novel function in improving metabolic disorders. Adv Sci (Weinh) 2024;11:e2309255.
23. Wang B, Shangguan W, Li W, et al. Blautia coccoides and its metabolic products enhance the efficacy of bladder cancer immunotherapy by promoting CD8(+) T cell infiltration. J Transl Med 2024;22:964.
24. Liu TC, Kern JT, Jain U, et al. Western diet induces Paneth cell defects through microbiome alterations and farnesoid X receptor and type I interferon activation. Cell Host Microbe 2021;29:988–1001.e6.
25. Sun H, Guo Y, Wang H, et al. Gut commensal Parabacteroides distasonis alleviates inflammatory arthritis. Gut 2023;72:1664–1677.
26. Zhao C, Wu K, Hao H, et al. Gut microbiota-mediated secondary bile acid alleviates Staphylococcus aureus-induced mastitis through the TGR5-cAMP-PKA-NF-κB/NLRP3 pathways in mice. NPJ Biofilms Microbiomes 2023;9:8.
27. Hu J, Wang C, Huang X, et al. Gut microbiota-mediated secondary bile acids regulate dendritic cells to attenuate autoimmune uveitis through TGR5 signaling. Cell Rep 2021;36:109726.
28. Fang D, Xu T, Sun J, et al. Nicotinamide mononucleotide ameliorates sleep deprivation-induced gut microbiota dysbiosis and restores colonization resistance against intestinal infections. Adv Sci (Weinh) 2023;10:e2207170.
29. Gao Q, Xu Y, Feng Y, et al. Deoxycholic acid inhibits ASFV replication by inhibiting MAPK signaling pathway. Int J Biol Macromol 2024;266:130939.
30. Jain U, Lai CW, Xiong S, et al. Temporal regulation of the bacterial metabolite deoxycholate during colonic repair is critical for crypt regeneration. Cell Host Microbe 2018;24:353–363.e5.
31. Xia Y, Xu X, Guo Y, et al. Mesenchymal stromal cells overexpressing farnesoid X receptor exert cardioprotective effects against acute ischemic heart injury by binding endogenous bile acids. Adv Sci (Weinh) 2022;9:e2200431.
32. Zheng Y, Sun W, Wang Z, et al. Activation of pancreatic acinar FXR protects against pancreatitis via Osgin1-mediated restoration of efficient autophagy. Research (Wash D C) 2022;2022:9784081.
33. Hartmann P, Hochrath K, Horvath A, et al. Modulation of the intestinal bile acid/farnesoid X receptor/fibroblast growth factor 15 axis improves alcoholic liver disease in mice. Hepatology 2018;67:2150–2166.
34. Xu H, Fang F, Wu K, et al. Gut microbiota-bile acid crosstalk regulates murine lipid metabolism via the intestinal FXR-FGF19 axis in diet-induced humanized dyslipidemia. Microbiome 2023;11:262.
35. Li DK, Chaudhari SN, Lee Y, et al. Inhibition of microbial deconjugation of micellar bile acids protects against intestinal permeability and liver injury. Sci Adv 2022;8:eabo2794.
36. Mullish BH, McDonald JAK, Pechlivanis A, et al. Microbial bile salt hydrolases mediate the efficacy of faecal microbiota transplant in the treatment of recurrent Clostridioides difficile infection. Gut 2019;68:1791–1800.
37. Joyce SA, MacSharry J, Casey PG, et al. Regulation of host weight gain and lipid metabolism by bacterial bile acid modification in the gut. Proc Natl Acad Sci U S A 2014;111:7421–7426.
38. Brinck JE, Sinha AK, Laursen MF, et al. Intestinal pH: a major driver of human gut microbiota composition and metabolism. Nat Rev Gastroenterol Hepatol 2025;22:639–656.
39. Banks PA, Bollen TL, Dervenis C, et al. Classification of acute pancreatitis–2012: revision of the Atlanta classification and definitions by international consensus. Gut 2013;62:102–111.
40. Kim E, Chang HC, Kim HY. Complete genome sequence of Lactobacillus plantarum EM, a putative probiotic strain with the cholesterol-lowering effect and antimicrobial activity. Curr Microbiol 2020;77:1871–1882.
41. Kumar R, Grover S, Batish VK. Bile salt hydrolase (Bsh) activity screening of lactobacilli: in vitro selection of indigenous lactobacillus strains with potential bile salt hydrolysing and cholesterol-lowering ability. Probiotics Antimicrob Proteins 2012;4:162–172.
42. Wen L, Voronina S, Javed MA, et al. Inhibitors of ORAI1 prevent cytosolic calcium-associated injury of human pancreatic acinar cells and acute pancreatitis in 3 mouse models. Gastroenterology 2015;149:481–492.e7.

Received September 6, 2025. Accepted January 12, 2026.

Correspondence
Address correspondence to: Yue Zeng, PhD, Department of Gastroenterology, Shanghai General Hospital, No. 650 Xinsongjiang Road, Songjiang District, Shanghai, China. e-mail: carrie_1004@sjtu.edu.cn; Chunlan Huang, PhD, Department of Gastroenterology, Shanghai General Hospital, No. 650 Xinsongjiang Road, Songjiang District, Shanghai, China. e-mail: chunlan.huang@shgh.cn; or Junjie Fan, PhD, Department of Gastroenterology, Shanghai General Hospital, No. 650 Xinsongjiang Road, Songjiang District, Shanghai, China. e-mail: 956937215@qq.com.

CRediT Authorship Contributions
Yang Fu (Data curation: Lead; Formal analysis: Lead; Investigation: Lead; Methodology: Lead; Writing – original draft: Lead)
Binqiang Xu (Data curation: Equal; Formal analysis: Equal; Methodology: Equal; Validation: Equal)
Wenfei Qin (Data curation: Equal; Formal analysis: Equal; Methodology: Equal; Resources: Equal)
Wei Xiao (Investigation: Supporting; Methodology: Supporting; Software: Supporting)
Huizhen Huang (Validation: Supporting; Visualization: Supporting)
Jia Hu (Formal analysis: Supporting; Methodology: Supporting)
Mengyan Cui (Software: Supporting; Visualization: Supporting)
Qixiang Mei (Methodology: Supporting; Writing – review & editing: Supporting)
Junjie Fan (Data curation: Equal; Formal analysis: Supporting; Investigation: Equal; Validation: Supporting; Writing – review & editing: Supporting)
Chunlan Huang (Project administration: Equal; Supervision: Equal; Writing – review & editing: Equal)
Yue Zeng (Conceptualization: Lead; Funding acquisition: Lead; Project administration: Lead; Supervision: Lead)

Conflicts of interest
The authors disclose no conflicts.

Funding
This work was supported by the National Natural Science Foundation of China (No. 82270671, 82300731, 82470675), Shanghai General Hospital (CCTR-2022B02), and Shanghai Municipal Health Commission (202440170).